NATIONAL ADVISORY COMMITTEE FOR AERONAUTICS

REPORT 1292

INTENSITY, SCALE, AND SPECTRA OF TURBULENCE IN MIXING REGION OF FREE SUBSONIC JET

By JAMES C. LAURENCE

1956

For sale by the Superintendent of Documents, U. S. Government Printing Office, Washington 25, D. C. Yearly subscription, $10; foreign, $11.25; single copy price varies according to size - Price 30 cents

REPORT 1292

INTENSITY, SCALE, AND SPECTRA OF TURBULENCE IN MIXING REGION OF FREE SUBSONIC JET

By JAMES C. LAURENCE

Lewis Flight Propulsion Laboratory
Cleveland, Ohio

National Advisory Committee for Aeronautics

Headquarters, 1512 H Street NW., Washington 25, D. C.

Created by act of Congress approved March 3, 1915, for the supervision and direction of the scientific study of the problems of flight (U. S. Code, title 50, sec. 151). Its membership was increased from 12 to 15 by act approved March 2, 1929, and to 17 by act approved May 25, 1948. The members are appointed by the President, and serve as such without compensation.

REPORT 1292

INTENSITY, SCALE, AND SPECTRA OF TURBULENCE IN MIXING REGION OF FREE SUBSONIC JET [1]

By James C. Laurence

SUMMARY

The intensity of turbulence, the longitudinal and lateral correlation coefficients, and the spectra of turbulence in a 3.5-inch-diameter free jet were measured with hot-wire anemometers at exit Mach numbers from 0.2 to 0.7 and Reynolds numbers from 192,000 to 725,000.

The results of these measurements show the following: (1) Near the nozzle (distances less than 4 or 5 jet diam downstream of the nozzle) the intensity of turbulence, expressed as percent of core velocity, is a maximum at a distance of approximately 1 jet radius from the centerline and decreases slightly with increasing Mach and/or Reynolds number. At distances greater than 8 jet diameters downstream of the nozzle, however, the maximum intensity moves out and decreases in magnitude until the turbulence-intensity profiles are quite flat and approaching similarity. (2) The lateral and longitudinal scales of turbulence are nearly independent of Mach and/or Reynolds number and in the mixing zone near the jet vary proportionally with distance from the jet nozzle. (3) Farther downstream of the jet the longitudinal scale reaches a maximum and then decreases approximately linearly with distance. (4) Near the nozzle the lateral scale is much smaller than the longitudinal and does not vary with distance from the centerline, while the longitudinal scale is a maximum at a distance from the centerline of about 0.7 to 0.8 of the jet radius. (5) Farther downstream this maximum moves out from the centerline. (6) A statistical analysis of the correlograms and spectra yields a "scale" which, although different in magnitude from the conventional, varies similarly to the ordinary scale and is easier to evaluate.

INTRODUCTION

Recent analyses by Lighthill (ref. 1) and by others (refs. 2 and 3) show that turbulence may be chiefly responsible for the noise from high-speed jets. However, a complete analysis relating turbulence to noise has not yet been made. Consequently, it is not known where the noise originates in the jet or which of the turbulence parameters, intensity, scale, or spectral distribution, is best suited to noise studies. Lighthill has suggested that each turbulent eddy might be considered as a single concentrated sound radiator. If Lighthill's suggestion is valid, it will be necessary to know the turbulence characteristics throughout the jet. The intensity of sound radiation will surely be related to the intensity of turbulence. Furthermore, the spectral distribution of turbulent energy might reasonably be expected to give information about the spectral distribution of sound energy.

Three regions of the jet need to be investigated (see fig. 1):

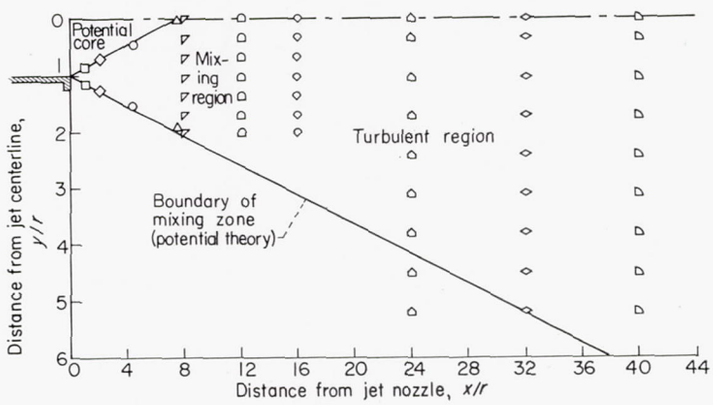

FIGURE 1.—Location of test points in subsonic jet.

(1) the central core, where the velocity profiles are flat and the intensity of the turbulent fluctuations is low; (2) the mixing region, which lies between the central core and the undisturbed air of the surroundings, where the velocity gradients are large and the intensity of turbulence is high; and (3) the region farther downstream where the central core and the mixing region blend into a completely turbulent airstream. The purpose of experiments in these regions is to measure the statistical parameters of the turbulence in the mixing zone and in the completely turbulent region of the jet.

Several investigators have reported the results of work in these regions (refs. 4 to 8). Reference 4 has only a limited amount of hot-wire data in the mixing zone, along with velocity-profile and turbulence-level measurements near the axis of the jet. Corrsin has made or has collaborated in making the most complete measurements in jets to be found in the literature (refs. 5 to 7). These investigations are of great interest and of much use, but the velocities investigated are small ($<$100 ft/sec). Hot-wire measurements in a unique form of a half-jet in which a solid wall replaces one side of the free mixing region are reported in reference 8.

In order to obtain data in speed ranges that are of more interest in jet noise research, a systematic investigation of the turbulent mixing region of a free jet was undertaken as part of the jet noise program at the NACA Lewis laboratory.

[1] Supersedes NACA Technical Notes 3561, "Intensity, Scale, and Spectra of Turbulence in Mixing Region of Free Subsonic Jet," by James C. Laurence, 1955; and 3576, "Further Measurements of Intensity, Scale, and Spectra of Turbulence in a Subsonic Jet," by James C. Laurence and Truman M. Stickney, 1956.

Principal interest was placed on measurements with the hot-wire anemometer of the statistical parameters of turbulence in the exit Mach number range from 0.2 to 0.7 and Reynolds numbers (based on jet radius) from 192,000 to 725,000. Since it was impossible to vary Mach numbers and Reynolds numbers independently, their combined effects are called Mach and/or Reynolds number effects herein.

The analysis of the results of these turbulence studies follows the statistical approach first introduced by Taylor (ref. 9). Dryden reviews this method in reference 10 and shows the success of this type of approach in dealing with isotropic turbulence. Similar approaches to the analysis of the results of studies of jet turbulence have been made also. But the results have not been very successful, especially in the mixing region of the jet. Hence, a statistical analysis is presented in this report which uses a different value of the "scale" or eddy size based on the energy spectrum of the turbulence.

INSTRUMENTATION AND TEST FACILITIES

HOT-WIRE ANEMOMETERS

The hot-wire anemometers used in this test were the constant-temperature anemometers described in reference 11. Constant-temperature anemometers were chosen instead of constant-current anemometers because of certain advantages: (1) The wire current is controlled by an electronic servosystem that protects against accidental wire burnout when the flow is suddenly reduced. (2) Since the bridge balance is maintained during flow changes, there are no compensation controls to set and no testing to determine whether the compensation is effective. (3) Finally, this instrument can follow large fluctuations in flow without appreciable error.

The hot-wire anemometer and the auxiliary equipment have been improved in several respects (see refs. 11 and 12). The direct-current amplifier has an improved frequency response, and its equivalent input noise has been decreased to

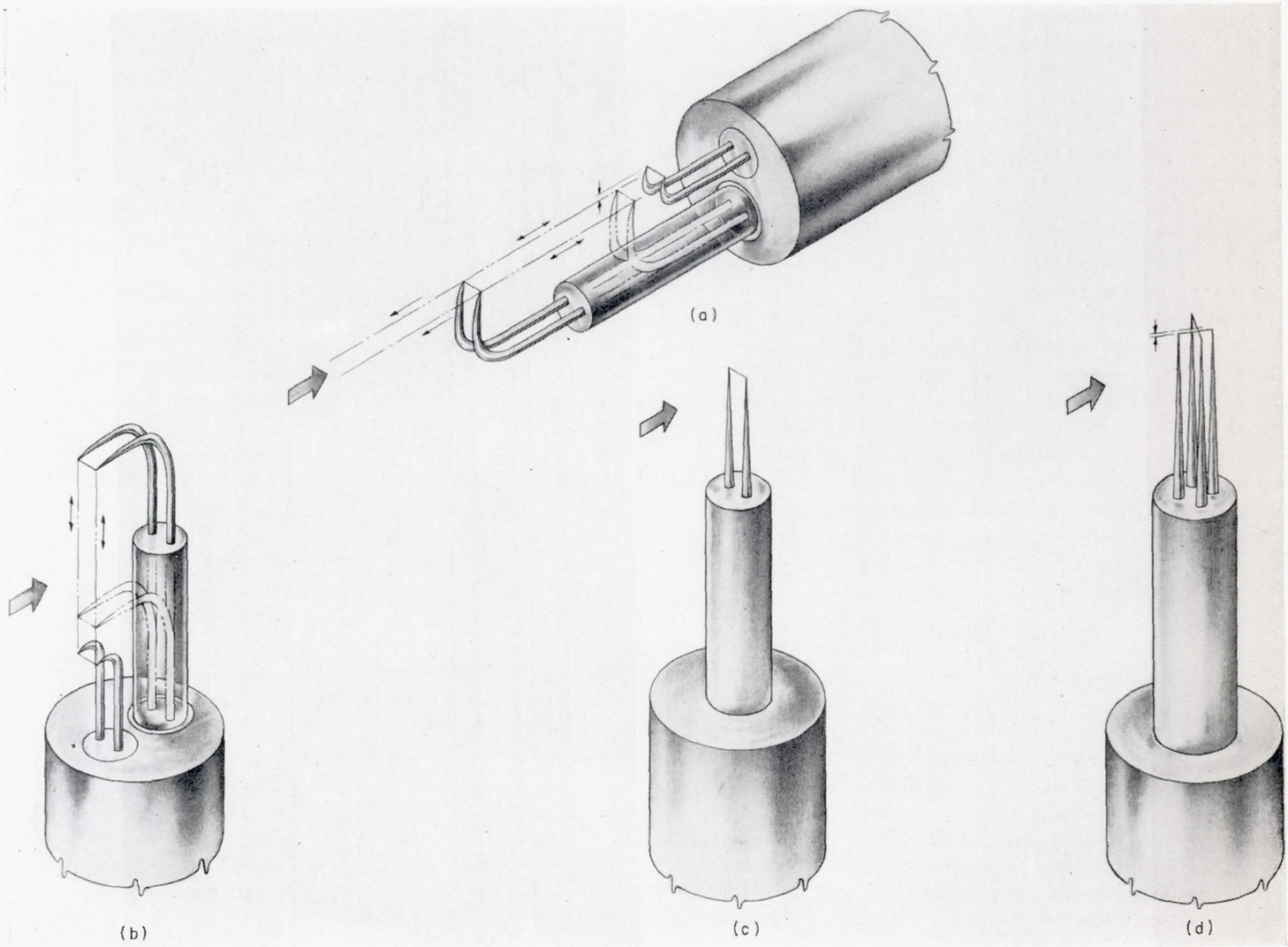

(a) Longitudinal correlation of velocity components in x-direction.

(b) Lateral correlation of velocity components in x-direction.

(c) Intensities and autocorrelations of velocity in x-direction.

(d) Velocity components in y-direction.

FIGURE 2.—Hot-wire-anemometer probes.

a value comparable with that of other hot-wire instruments (less than 100 microvolts). Frequency-response measurements made according to the methods described in reference 11 show an over-all response (amplifier, bridge, wire, and cables) of about 100 kilocycles.

HOT-WIRE PROBES

The hot-wire probes (fig. 2) were single- and double-wire probes. The double-wire probes were arranged in parallel and X-array. The parallel arrays (figs. 2(a) and (b)) were used to measure the longitudinal and lateral u velocity correlation coefficients, respectively. For the longitudinal correlations one wire was held fixed and the other was moved downstream. This wire was displaced not more than 0.005 inch towards the centerline of the jet to avoid interference from the flow over the first wire. A similar arrangement was used for the lateral correlations. Practical limitations on the separability of the wires limited the number of points for which measurements could be obtained. The measured correlations were assumed to be those at the position of the fixed wire. The X-array (fig. 2(c)) was employed to measure the v-component of the velocity fluctuations. The single-wire probe (fig. 2(d)) measured the u velocity intensities and all autocorrelations.

The wire material used in the tests was the 0.0002-inch tungsten wire evaluated in reference 11. The mounting procedure is an adaptation of the plating-soldering technique that was first used by the National Bureau of Standards (ref. 13).

SPECTRUM ANALYZERS

Two spectrum analyzers were used in obtaining the spectral density data. One of these has a constant narrow band pass (5 cps) with a frequency response from 20 to 16,000 cps; the other is a constant-percentage band-pass instrument with about the same frequency response. The filter characteristics of the two instruments are given in figure 3. The two analyzers give comparable spectral density curves within the general accuracy of the experiments.

TAPE RECORDER

A dual-channel tape recorder was used to record the signals from a single hot-wire-anemometer probe located in the airstream. These recordings were later used to obtain the autocorrelation coefficients.

ACTUATORS

The lateral positions of the probe were controlled by screw-type actuators. The longitudinal positions, however, were set by adjustments of a lathe carriage. The probes were alined in the stream with reference to the centerline of the jet. This aerodynamic centerline was determined from total-pressure measurements in the jet. A plug was machined to fit the exit nozzle of the jet, and a steel wire was stretched along the centerline to a point on the centerline far downstream in the jet (approx. 12 ft). A telescope mounted at this point helped in relocating the probes after a probe failure without restringing the steel wire.

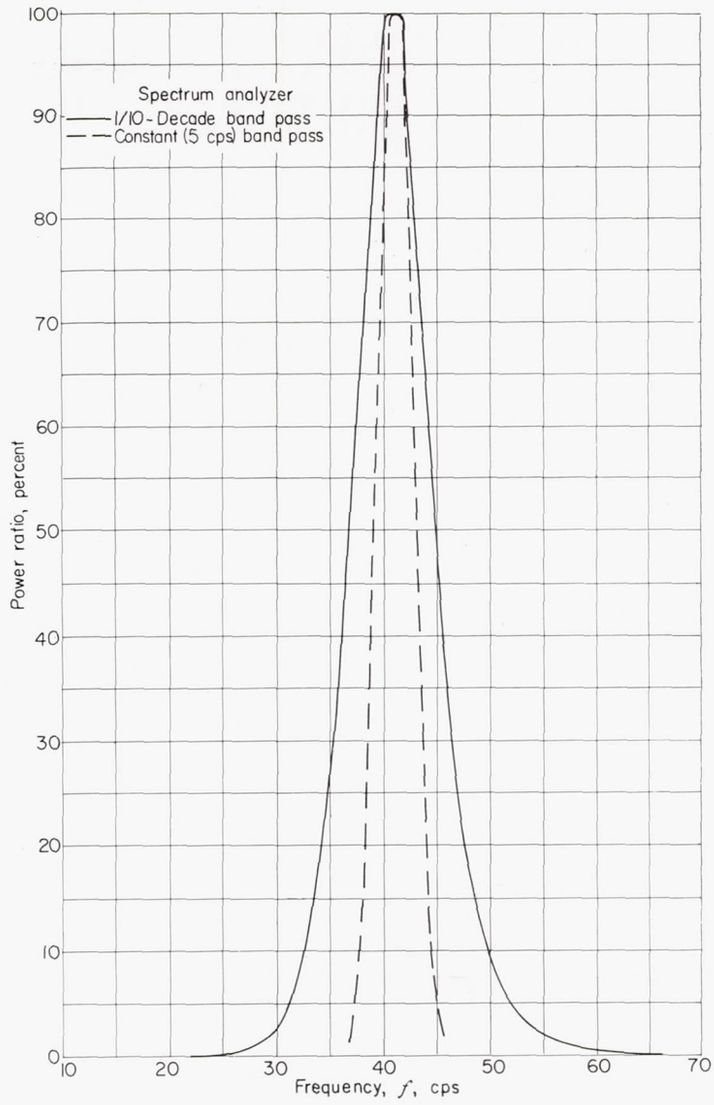

FIGURE 3.—Band-pass filter characteristics.

TEST FACILITIES

The subsonic jet and associated plenum chamber used in these experiments are shown schematically in figure 4. The jet has a 3.5-inch-diameter nozzle at the end of a bell-

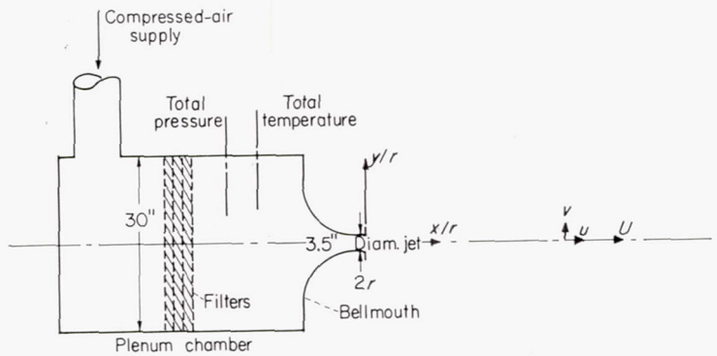

FIGURE 4.—Schematic diagram of subsonic jet, plenum chamber, filters, and location of pressure- and temperature-measuring instruments.

mouth which is attached to a large plenum chamber. The turbulence intensity in the plenum chamber varied from 4 to 5 percent over the range of the test conditions. The whole is connected to a compressed-air supply. A filter is included as an integral part of the plenum chamber. It successfully removes a large part of the dust and pipe scale sometimes found in similar airstreams. The flow is adjusted by means of electrically controlled valves throughout the subsonic range of Mach numbers. The instruments for measuring total pressure and temperature are placed in the plenum chamber and read remotely. Figure 1 shows the approximate location of the testing points in the jet, and table I gives the exact coordinates.

TABLE I.—LOCATION OF TEST POINTS IN SUBSONIC JET

Distance from jet nozzle, x/r	Distance from jet centerline, y/r								
1.14	1.206	1.154	1.103	1.051	1.00	0.949	0.846	0.794	0.743
2.29	----	1.308	1.206	1.103	1.00	.897	.794	.692	----
4.58	----	1.411	1.206	----	1.00	.794	.589	.383	----
7.6	----	1.686	1.500	1.343	1.00	.657	.314	−.029	----
8	----	2.000	1.714	1.286	1.00	.714	.286	0	----
12	----	2.00	1.714	1.286	1.00	.714	.286	0	----
16	----	2.00	1.714	1.286	1.00	.714	.286	0	----
24	5.143	4.460	3.772	3.088	2.400	1.715	1.028	.343	0
32	5.143	4.460	3.772	3.088	2.400	1.715	1.028	.343	0
40	5.143	4.460	3.772	3.088	2.400	1.715	1.028	.343	0

EXPERIMENTAL PROCEDURE

INTENSITY MEASUREMENTS

A single hot wire was used to measure the u-component of the turbulent intensity. An X-wire probe was used to measure the v-component. The hot-wire signal (or the instantaneous difference between the two X-wires) was measured directly by a root-mean-square voltmeter. Reference 11 describes the root-mean-square voltmeter (average-square computer) which was used in an improved form for the first half of the intensity surveys made. A true rms voltmeter was used for the remainder of the data. It gives a precise wide-band squaring action that is unaffected by normal ambient temperature variations and, in general, is more satisfactory than the other instrument.

The turbulence intensity was calculated by methods outlined in references 11, 13, and 14.

CORRELATION MEASUREMENTS

Velocity correlations in space and in time are of interest in the noise problem. Two hot wires can be used to obtain the lateral and longitudinal correlations. The wires are mounted on telescoping tubes that can be displaced either laterally or longitudinally with respect to each other by actuators. During the actual measurements, the fluctuating components of the two hot-wire signals, say ϵ_1 and ϵ_2, are led to a correlator that measures $\overline{\epsilon_1\epsilon_2}$, $\overline{\epsilon_1^2}$, and $\overline{\epsilon_2^2}$.

If a linear relation between the velocity fluctuation and the hot-wire voltage is assumed, that is,

$$\left.\begin{aligned} u_1 &= k_1\epsilon_1 \\ u_2 &= k_2\epsilon_2 \end{aligned}\right\} \tag{1}$$

as is done in reference 15, there results, upon combining the signals,

$$\mathcal{R} = \frac{\overline{u_1 u_2}}{\sqrt{\overline{u_1^2}}\sqrt{\overline{u_2^2}}} \tag{2}$$

$$\mathcal{R} = \frac{k_1 k_2 \overline{\epsilon_1\epsilon_2}}{\sqrt{k_1^2\overline{\epsilon_1^2}}\sqrt{k_2^2\overline{\epsilon_2^2}}} \tag{3}$$

$$= \frac{\overline{\epsilon_1\epsilon_2}}{\sqrt{\overline{\epsilon_1^2}}\sqrt{\overline{\epsilon_2^2}}} \tag{4}$$

(All symbols are defined in appendix A.)

The displacement of the wires in the lateral direction gives the lateral correlation coefficient; in the longitudinal, the longitudinal correlation coefficient.

An autocorrelation coefficient, that is, the correlation between two segments of the same signal separated in time, can be obtained if some method is devised to obtain from the signal of a single hot wire another signal delayed in time with respect to the first. An instrument that provides time delays of this nature (described in refs. 16 and 17) was designed and built at the NACA Lewis laboratory (ref. 18).

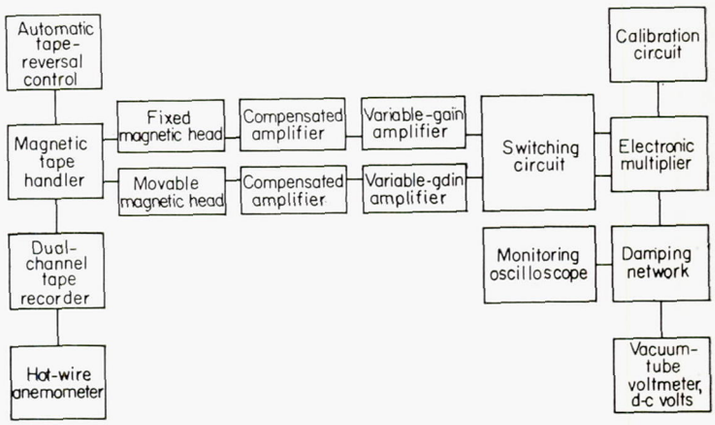

FIGURE 5.—Block diagram of correlation computer.

In general, this correlator (see fig. 5) works as follows: The signal from a single hot wire is recorded simultaneously on two channels of a dual-channel tape recorder. A special playback instrument uses two pickup heads, one of which can be displaced with respect to the other by means of a micrometer screw. When the two heads are in such a position that they are picking up identical signals, the correlation between these signals is necessarily unity. But if the movable head is displaced so that it is picking up a signal recorded a short time earlier or later, the two signals are, of course, different. These two signals are the two voltages ϵ_1 and ϵ_2 considered in equation (1). The correlation coefficient $\mathcal{R}$ is then the autocorrelation coefficient $\mathcal{R}_t$.

The value of the time interval Δt is obtained from the actual displacement of the head and the constant tape speed:

$$\Delta t = \frac{d}{S} \tag{5}$$

It is rather obvious that there should be a relation between the autocorrelation and the longitudinal correlation coefficients involving the stream velocity U and the head separation (ref. 19).

An extension of this method can be made to measure the autocorrelation of the v-components of the turbulence. In this method the difference signal from an X-wire probe

located in the stream is recorded simultaneously on both channels of the recorder and played back in the usual way.

The double correlator of reference 11 was used to obtain correlations of the hot-wire signals for the first half of the program. The ratios were calculated numerically, because the ratio meters that are sometimes used are unreliable. Inaccuracy results from the use of an average-square computer, which depends upon the operating characteristics of a vacuum tube to obtain the square of the sum and of the difference of two voltages in order to apply the quarter-square principle of multiplication.

After about half the data were obtained, an electronic multiplier replaced the double correlator. This multiplier (described in ref. 18) does not use the quarter-square principle of multiplication. The multiplier operates from d.c. to 50 kilocycles (3-db point) and is useful in obtaining correlation coefficients. Two channels are available to give the average product of two input voltages as well as their average squares. The outputs can be read on any high-impedance d-c voltmeter. By properly adjusting the level of the inputs, the correlation coefficients can be read directly.

SPECTRUM OF TURBULENCE

If the hot-wire signal is analyzed by means of a series of band-pass filters, a spectrum results. The relative energy spectrum is more fully discussed in references 10 and 20. Most of the spectra presented here were recorded on a paper strip chart by an analyzer of constant percentage (1/10-decade) band width. The switching from one filter to the next is done automatically and in synchronization with the movement of the chart. The spectrum recordings are made rapidly (about 1 per min) and with little attention by the operator.

The chart recordings are in decibels above any practical reference voltage, and at one point on the chart the total voltage level for the entire range of frequencies is recorded. The conversion to spectral density is as follows: By definition,

$$\left.\begin{aligned} N_b &= 20 \log \frac{\epsilon_{w,b}}{\epsilon_{ref}} \\ N_{tot} &= 20 \log \frac{\epsilon_{w,tot}}{\epsilon_{ref}} \end{aligned}\right\} \tag{6}$$

Therefore,

$$\left.\begin{aligned} \frac{\epsilon_{w,b}}{\epsilon_{ref}^2} &= \text{antilog} \frac{N_b}{10} \\ \frac{\epsilon_{w,tot}^2}{\epsilon_{ref}^2} &= \text{antilog} \frac{N_{tot}}{10} \end{aligned}\right\} \tag{7}$$

Hence, the spectral density function

$$\mathcal{F}(f) = \frac{1}{B} \frac{\text{antilog} \frac{N_b}{10}}{\text{antilog} \frac{N_{tot}}{10}} \tag{8}$$

where B is the band-pass width of the filters.

The resulting display of the spectral density function with frequency shows the content of the signal in each individual frequency band. This method of analysis is important for two reasons: (1) It tells the experimenter the frequency bands in which most of the energy is concentrated, and (2) the spectrum can be used to obtain the average eddy size.

SCALE OF TURBULENCE

The scales of turbulence $\mathcal{L}$ (ref. 21) are defined in many applications as follows:

Longitudinal:

$$\mathcal{L}_x = \int_0^\infty \mathcal{R}_x \mathrm{d}x \tag{9a}$$

Lateral:

$$\mathcal{L}_y = \int_0^\infty \mathcal{R}_y \mathrm{d}y \tag{9b}$$

$$\mathcal{L}_z = \int_0^\infty \mathcal{R}_z \mathrm{d}z \tag{9c}$$

If

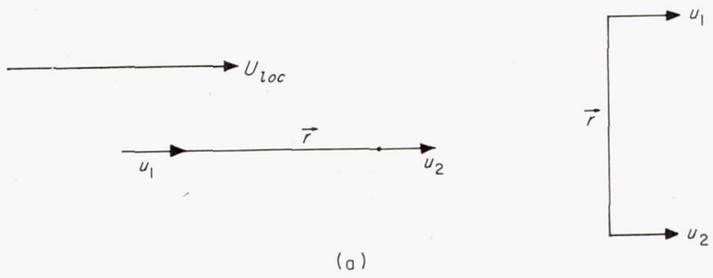

(a)

then

$$\mathcal{L}_x = \int_0^\infty \frac{\overline{u_1 u_2}}{\sqrt{\overline{u_1^2}}\sqrt{\overline{u_2^2}}} \mathrm{d}r$$

These scales are generally regarded as the physical dimensions in the x- (longitudinal), y- (radial), and z- (tangential) directions of the average eddy in the flow. The three scales, as defined in equations (9), are all important in a study of jet noise. However, variations in the tangential direction are not included in this report. Reference 21 shows that the correlation coefficient $\mathcal{R}$ is related to the spectral density as follows:

$$\mathcal{R}_x = \int_0^\infty \mathcal{F}(f) \cos \frac{2\pi f x}{U} \mathrm{d}f \tag{10}$$

and, inversely,

$$\mathcal{F}(f) = \frac{4}{U} \int_0^\infty \mathcal{R}_x \cos \frac{2\pi f x}{U} \mathrm{d}x \tag{11}$$

Thus, there are two possible ways to obtain the longitudinal correlation coefficient. One is to measure it directly; the other is to obtain it from the turbulence spectrum and equation (10). If the longitudinal correlation coefficient $\mathcal{R}_x$ is assumed to be exponential in form, that is,

$$\mathcal{R}_x = e^{-x/\mathcal{L}_x} \tag{12}$$

then the transform (eq. (11)) can be readily worked out as (ref. 10)

$$\mathcal{F}(f) = \frac{\frac{4\mathcal{L}_x}{U}}{1 + \left(\frac{2\pi \mathcal{L}_x f}{U}\right)^2} \tag{13}$$

Analogous relations are available for the transverse correlations.

The methods just outlined have been used to great advantage in the analysis of turbulence induced by grids in wind tunnels (ref. 21). Similar application to the flow in subsonic jets does not prove to be so successful, however, particularly in the mixing region close to the nozzle of the jet, since the definitions do not apply to shear flows.

In particular, the correlograms that resulted from the two-wire measurements and the autocorrelation measurements in the jet are not fitted very well by a single exponential. A typical correlogram is shown in figure 6(a). It is apparent that the shape of this curve is different from a pure exponential. In order to find a curve of best fit for this data, a function was built up which is the algebraic sum of two exponentials, as shown in figure 6(b). The correlation fitting function is then of the following form (see appendix B):

$$\mathcal{R}_x=\frac{e^{-x/\Lambda_x}-\beta e^{-\beta x/\Lambda_x}}{1-\beta} \tag{14a}$$

or

$$\mathcal{R}_t=\frac{e^{-\omega^* t}-\beta e^{-\beta\omega^* t}}{1-\beta} \tag{14b}$$

In these equations the constants β, Λ_x, and ω^* have specialized meanings. The Λ_x is a characteristic eddy size that is different in magnitude from the longitudinal scale of the turbulence $\mathcal{L}_x$, and ω^* is related to this eddy size by $\omega^*=U/\Lambda_x$. The parameter β is related to the cut-off frequencies (upper and lower) of the spectral density curves by the relation

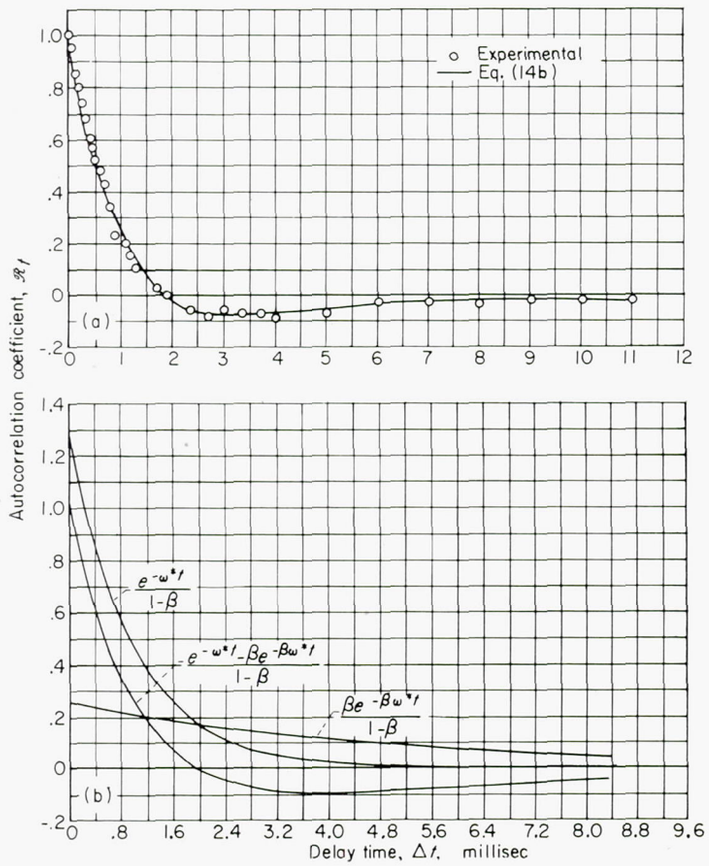

(a) Typical autocorrelogram.
(b) Method used to approximate autocorrelograms.

FIGURE 6.—Autocorrelograms; $\beta=0.2$; $\omega^*=6283$ radians per second.

$$\frac{f_l}{f_u}=\frac{\beta}{(1+\beta)^2}$$

The cut-off frequency is defined in the usual electronic sense as the intersection of the asymptotes of the spectral density curve with a horizontal line through the maximum point of the spectral density curve. The relation between the distance x and the time t in these experiments is the velocity of the stream; that is (ref. 20),

$$x=U_{loc}t \tag{15}$$

Equations (14) can be adjusted by means of the quantities Λ_x, β, and ω^* to fit the correlograms obtained experimentally.

It is now obvious that the conventional definition of the scales of the turbulence (eqs. (9)) is no longer valid, since the integral is always zero if $\mathcal{R}$ has the form of equations (14). The parameter β, however, is useful in obtaining a measure of the eddy size, which, after all, is what is meant by the scale of the turbulence. In equation (14a), if $\mathcal{R}_x=0$,

$$\Lambda_x=\frac{x_0(\beta-1)}{\ln\ \beta} \tag{16}$$

where x_0 is the value of the wire separation when $\mathcal{R}_x$ is first equal to zero. This definition of scale is related to two quantities that are quite easy to evaluate from the experimental correlograms and spectra: (1) the first crossing of the abscissa by the correlation curve, and (2) the parameter β, which is related to the ratio of the low- to the high-frequency cut-off of the spectral density curves.

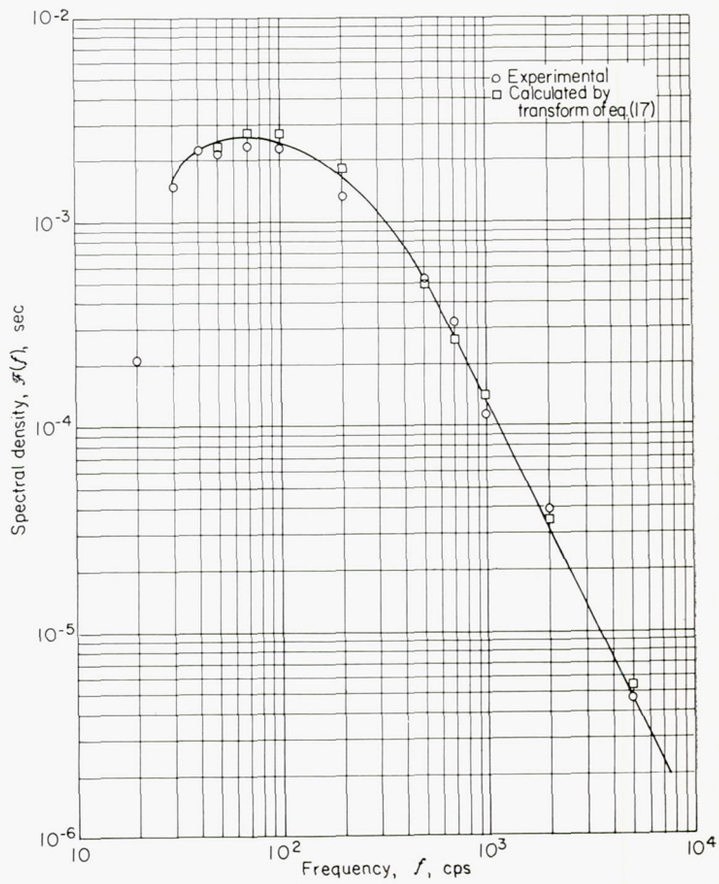

FIGURE 7.—Typical spectral density curve.

The transform of equation (14a) can be obtained with the following result:

$$\mathcal{F}(f)=\frac{1+\beta}{4f^*}\frac{\left(\frac{f}{f^*}\right)^2}{\left[1+\left(\frac{f}{f^*}\right)^2\right]\left[\beta^2+\left(\frac{f}{f^*}\right)^2\right]} \tag{17}$$

where β is the same as in equations (14), and

$$f^*=\frac{\omega^*}{2\pi} \tag{18}$$

Figure 7 shows a typical spectral density curve obtained in the completely turbulent region of a subsonic jet. It represents data obtained at the same time and at the same location in the same jet as the correlogram of figure 6(a). A spectrum fitting function of the type of equation (17) was calculated by the methods described in appendix B from the correlation curve. These calculated points are shown for comparison with the experimentally obtained spectrum.

ACCURACY OF MEASUREMENTS

The accuracy of the hot-wire measurements made with the constant-temperature instrument is discussed in references 11 and 12. It is sufficient to say here that these measurements are made as accurately as the usual hot-wire measurements. In measuring quantities that vary randomly with time, a certain amount of discretion must be used in obtaining averaged readings of meter pointers that are jumping about. Reference 12 includes an evaluation of the NACA Lewis laboratory hot-wire equipment and experimental techniques and compares them with other systems.

No corrections have been made to any of the hot-wire results for the finite length of the wire. In these measurements, the scales of turbulence were much greater than the length of the hot wires (0.080 and 0.040 in.).

Some of the intensities measured were large compared with the local mean flow. In the constant-temperature method of anemometry, these large intensities can be evaluated (see appendix F, ref. 11). In the usual method and in the method used herein, however, the root mean square of the voltage fluctuations is used in place of their instantaneous values. This approximation is valid only for small values of the fluctuations. Nevertheless, vibration studies (e. g., ref. 5) have shown that the hot-wire anemometer itself is capable of following fluctuations in a single direction faithfully up to 60 to 70 percent.

When the fluctuations in U become large, errors will be introduced because of the interaction of the components of the turbulence; that is, the effect of u, v, and w on U and on

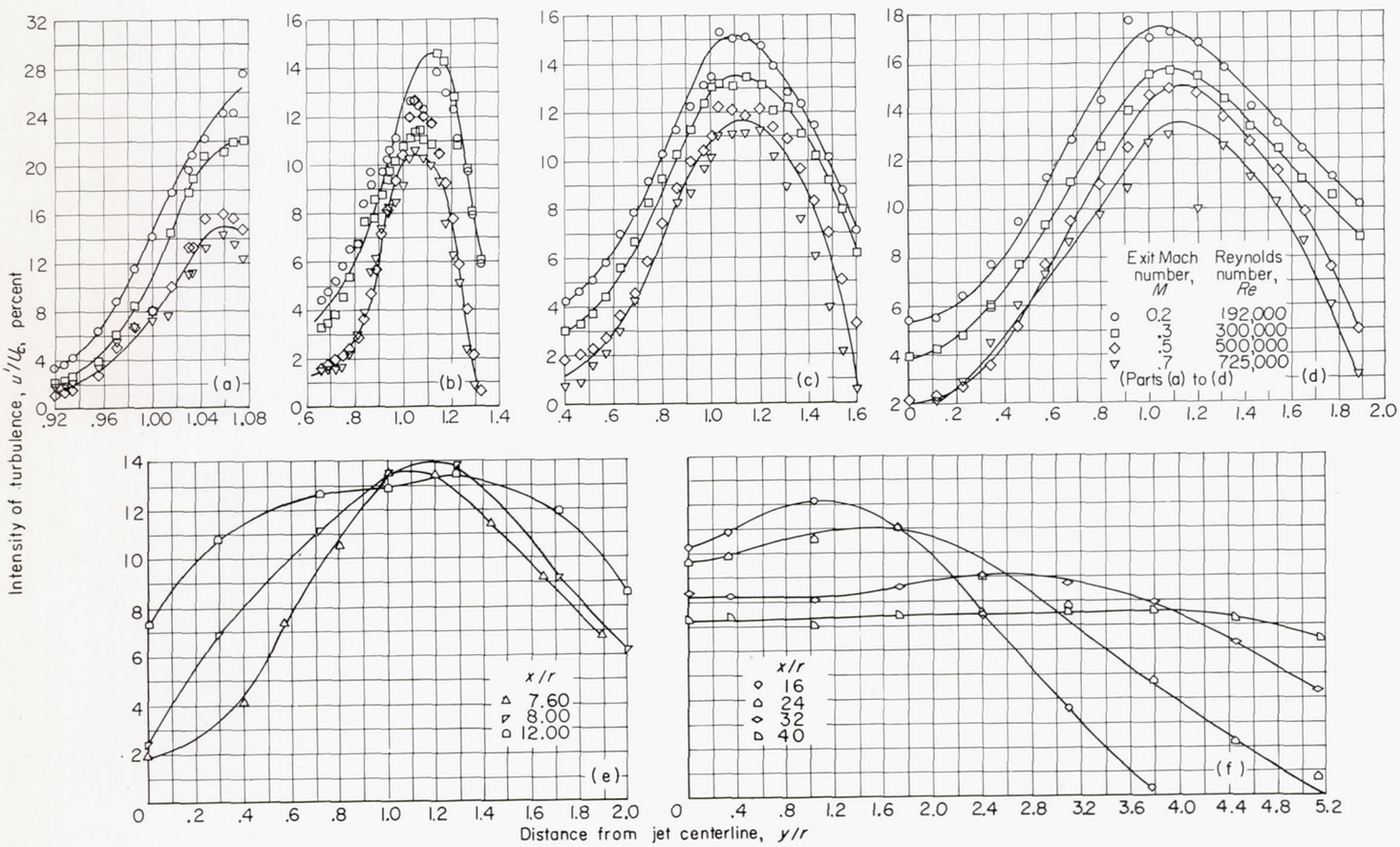

(a) Distance from jet nozzle x/r, 1.14.

(b) Distance from jet nozzle x/r, 2.29.

(c) Distance from jet nozzle x/r, 4.58.

(d) Distance from jet nozzle x/r, 7.60.

(e) Distance from jet nozzle x/r, 7.60, 8, and 12. Exit Mach number, 0.3; Reynolds number, 300,000.

(f) Distance from jet nozzle x/r, 16 to 40. Exit Mach number, 0.3; Reynolds number, 300,000.

FIGURE 8.—Intensity of turbulence in percent of core velocity at various exit Mach and/or Reynolds numbers.

each other. These errors are considered in reference 12, where actual corrections are worked out. No such corrections have been applied to the results shown in this report.

Some of the correlations measured with the average-square computer and the sum and difference circuits (quarter-square multiplication) show values greater than unity. This is, of course, impossible, and such readings must be the result of inaccuracies in the multiplication. In most of these instances enough points are available to fair a reasonable curve without considering these points ($\mathcal{R}>1$).

The largest sources of error in these experiments were (1) the inaccuracy in repeating setups after probes were changed, (2) the fluctuations in pressure in the air supply, which caused fluctuations in the mean flow level, and (3) the presence in the flow of periodic fluctuations due to sound or pressure waves and floor vibrations. It is believed that the measurements reported herein for turbulence intensities less than 30 percent are not in error by more than ± 10 percent.

RESULTS AND DISCUSSION

The results of these hot-wire measurements are presented in a series of graphs and tables. In general, the points for which the measurements are reported are shown in figure 1 and are tabulated in table I. However, for the intensity surveys many more points were used. For some of the correlation measurements, physical limitations in the amount of wire separation made it impossible to obtain results at all the points indicated in figure 1.

The order in which the results are presented has no special significance. The surveys are given for only one-half of the jet, because the jet was found to be essentially axisymmetric.

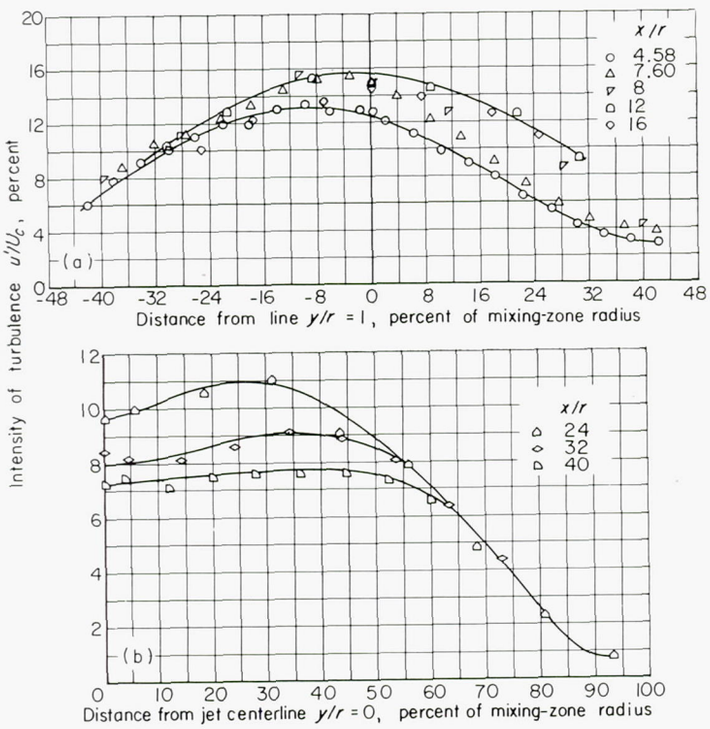

(a) Distances from jet nozzle less than 12 jet radii.
(b) Distances from jet nozzle greater than 24 jet radii.

FIGURE 9.—Similarity of turbulence-intensity profiles. Exit Mach number, 0.3; Reynolds number, 300,000.

INTENSITY OF TURBULENCE

The intensity measurements were made at values of the nondimensional radius y/r distributed across the mixing zone for several positions downstream of the jet nozzle. The results of these measurements are shown in figures 8 to 10. In figures 8(a), (b), (c), and (d), the turbulence intensity in percent of central-core velocity is presented for x/r values of 1.14, 2.29, 4.58, and 7.60, respectively, for four Mach numbers (0.2, 0.3, 0.5, and 0.7). In figures 8(e) and (f), the intensity is shown only for a Mach number of 0.3 at x/r values of 7.60, 8, 12, 16, 24, 32, and 40.

One point of particular interest is shown by figure 9. Figure 9(a) shows that the turbulence-intensity profiles near the jet nozzle (where the potential core is still present) are similar in shape and little different in actual magnitude of the intensity of turbulence. As the distance from the nozzle increases, however, this similarity disappears only to develop again in a different form far downstream. Figure 9(b) shows the reappearance of a degree of similarity, especially at points removed from the centerline of the jet. Here the turbulent velocity profiles are becoming quite flat for a large part of the mixing zone, the maximum value of the intensity moving out from the jet centerline. Figures 10(a) to (d) show the intensity of turbulence in percent of local mean velocity for the same Mach numbers and the same x/r values as figures 8(a) to (d).

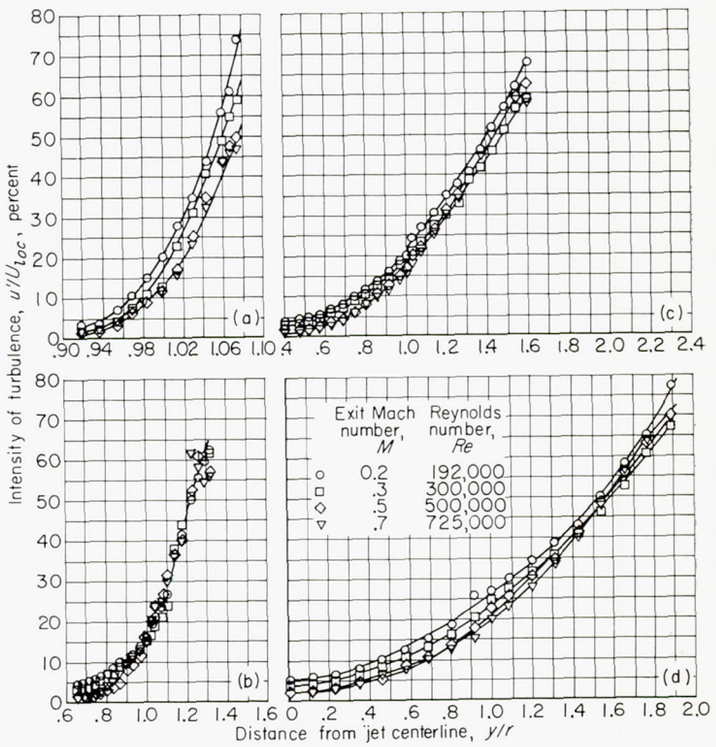

(a) Distance from jet nozzle x/r, 1.14.
(b) Distance from jet nozzle x/r, 2.29.
(c) Distance from jet nozzle x/r, 4.58.
(d) Distance from jet nozzle x/r, 7.60.

FIGURE 10.—Intensity of turbulance in percent of local velocity at various exit Mach and/or Reynolds numbers.

The mean velocity profiles (obtained from total-pressure surveys) are shown in figure 11. The local mean velocity in terms of central-core velocity is plotted against the nondimensional radius y/r for the entire range of Mach numbers and x/r values up to 40.

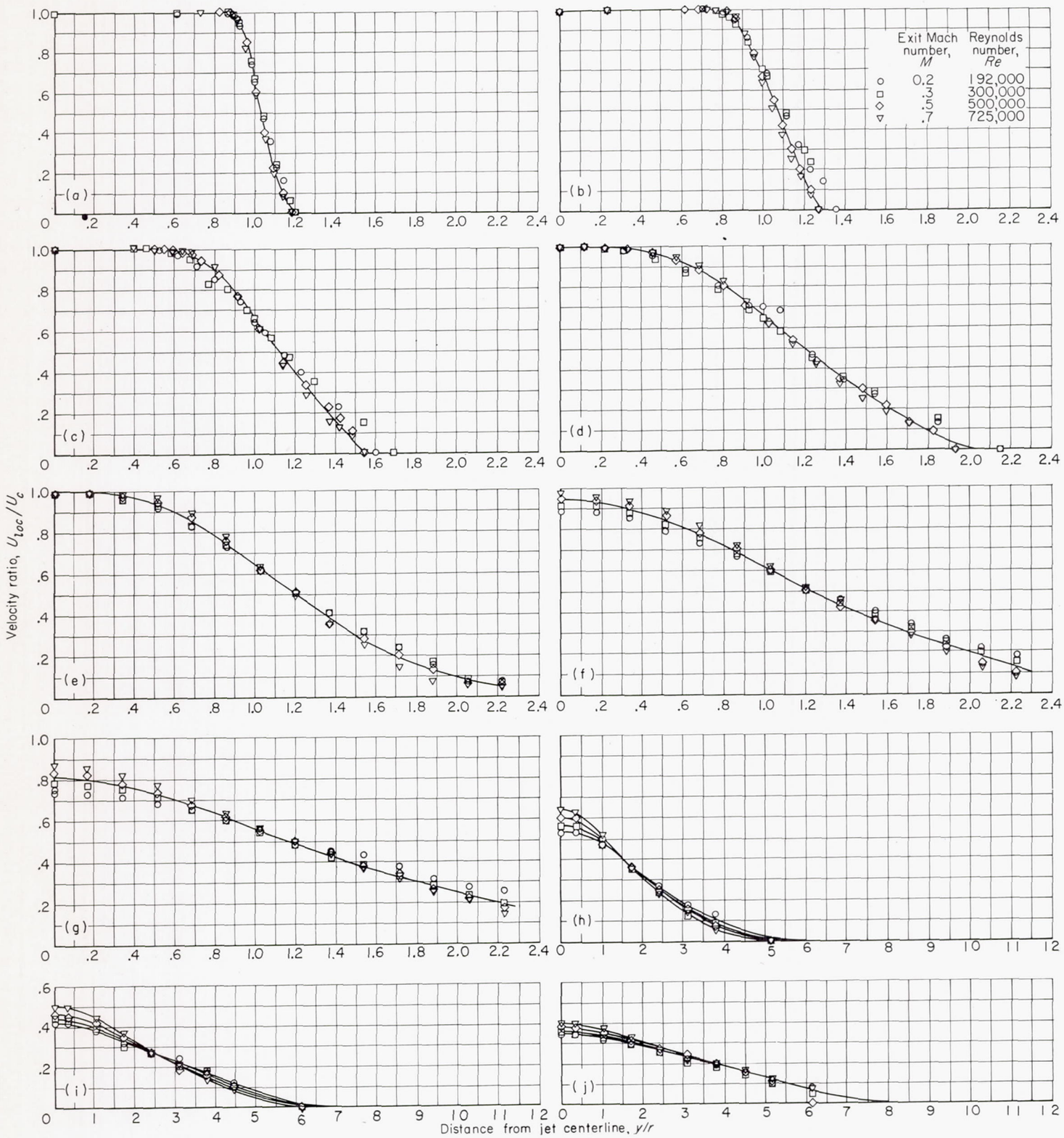

(a) Distance from jet nozzle x/r, 1.14.
(b) Distance from jet nozzle x/r, 2.29.
(c) Distance from jet nozzle x/r, 4.58.
(d) Distance from jet nozzle x/r, 7.60.
(e) Distance from jet nozzle x/r, 8.
(f) Distance from jet nozzle x/r, 12.
(g) Distance from jet nozzle x/r, 16.
(h) Distance from jet nozzle x/r, 24.
(i) Distance from jet nozzle x/r, 32.
(j) Distance from jet nozzle x/r, 40.

FIGURE 11.—Mean velocity profiles.

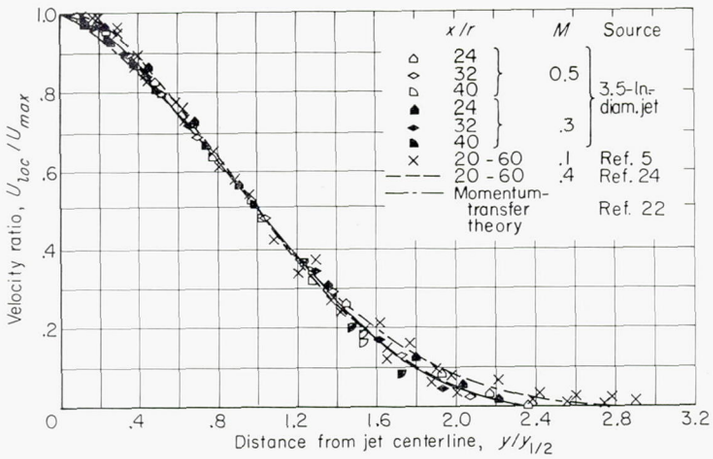

FIGURE 12.—Similarity of velocity profiles in region of fully developed flow. ($y_{1/2}$ is distance from axis where $U_{loc}=\frac{1}{2}U_{max}$.)

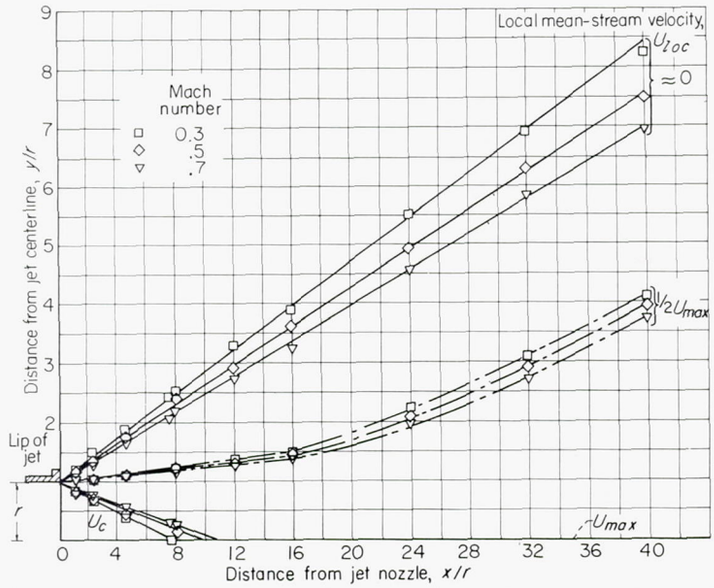

FIGURE 13.—Effect of potential-core Mach number on boundaries of 3.5-inch-diameter jet.

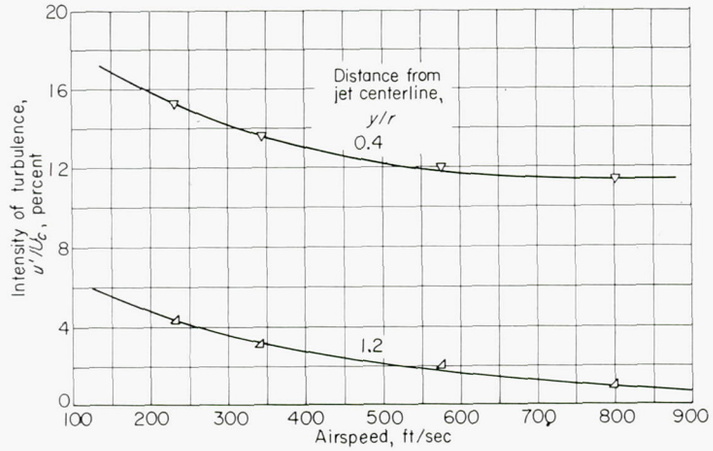

FIGURE 14.—Variation of intensity of turbulence with airspeed for circular nozzle. Distance from nozzle x/r, 4.58.

The mean velocity profiles are also similar, as is shown in figure 12, where the ratio of the local mean velocity to the maximum mean velocity is plotted against a nondimensional mixing-zone width. This width is defined as the ratio of the distance from the jet centerline to the point where the local velocity is half the maximum velocity. The figure shows very well the degree of similarity for all distances from the jet nozzle as well as for the different Mach numbers. Also shown is a comparison with the theoretical momentum-transfer results as given by reference 22.

The result of these mean velocity studies is shown in figure 13, where the approximate jet boundaries are shown for the different Mach numbers. The positions of the zero velocity, the one-half maximum, and the core velocity are shown.

A comparison of figures 8 and 11 shows that the maximum intensity occurs near the points of inflection of the velocity profiles at approximately 1 jet radius from the centerline for distances from the jet nozzle up to about 10 jet radii. As the distance from the nozzle increases, however, this position of the maximum intensity begins to move out from the jet centerline, and similarity of the profiles tends to develop far downstream from the nozzle. The curves show that the line of maximum shear moves out from the centerline as the distance downstream of the jet nozzle increases.

The observed turbulence levels decreased with increasing Mach and/or Reynolds number throughout the jet. Figure 14 shows that the level of turbulence in the central core and at the position of maximum intensity decreased with increasing exit Mach and/or Reynolds number. It is not clear, however, that the turbulence which is generated in the jet mixing process would change with jet Mach number if there were no initial turbulence in the jet. The decrease in intensity shown for the core may possibly explain the decrease noted in the mixing zone. If this explanation is accepted, the results of the intensity surveys are in a fair agreement with those reported in references 5 and 8.

The turbulence intensity of the v-component of the velocity fluctuations was measured at four points in the jet. These measurements, along with the corresponding u intensities, are included in table II. This table shows that the u and v intensities are not equal but may differ by about as much as 17 percent.

TABLE II.—COMPARISON OF u AND v INTENSITY MEASUREMENTS

x/r	y/r	$\frac{\sqrt{\overline{u^2}}}{U_{loc}}$	$\frac{\sqrt{\overline{v^2}}}{U_{loc}}$	Difference [a], percent
6	1.00	0.241	0.242	0.4
6	0	.101	.118	16.8
8	1.00	.266	.241	−10.4
8	0	.148	.134	−10.4

[a] Difference is in percent of smaller intensity.

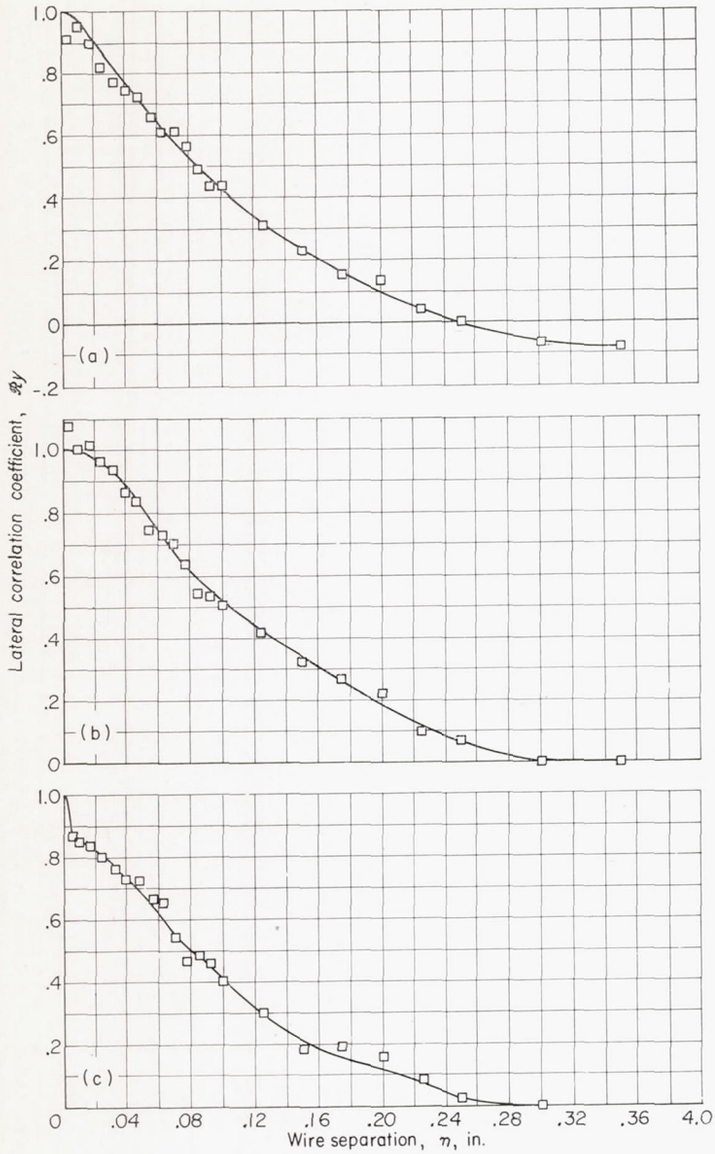

(a) Distance from jet centerline y/r, 1.065.
(b) Distance from jet centerline y/r, 1.00.
(c) Distance from jet centerline y/r, 0.935.

FIGURE 15.—Lateral velocity correlations. Distance from jet nozzle x/r, 1.14; exit Mach number, 0.3; Reynolds number, 300,000.

LATERAL CORRELATION COEFFICIENTS

For each distance from the jet nozzle x/r, three different distances from the jet centerline y/r were used in the measurement of lateral correlation coefficients for all the Mach numbers investigated At positions downstream greate · than approximately 1 jet diameter, the wires on the probes could not be separated far enough to reach zero correlation. Figures 15 and 16 are typical of the results for the lateral correlation coefficients. Figure 15 shows the variation of the lateral correlation for x/r of 1.14 and for three y/r values. Figure 16 shows the lateral correlation for y/r of 1.00 at several x/r values. Also shown on the curves of figure 16 are exponential curves that have been fitted to the data. The agreement is good for x/r values of 7.60 and 4.58 but only fair for x/r of 2.29 and 1.14. In some cases, however, this agreement justifies the use of equation (12) to obtain equation (13) for the spectral density function.

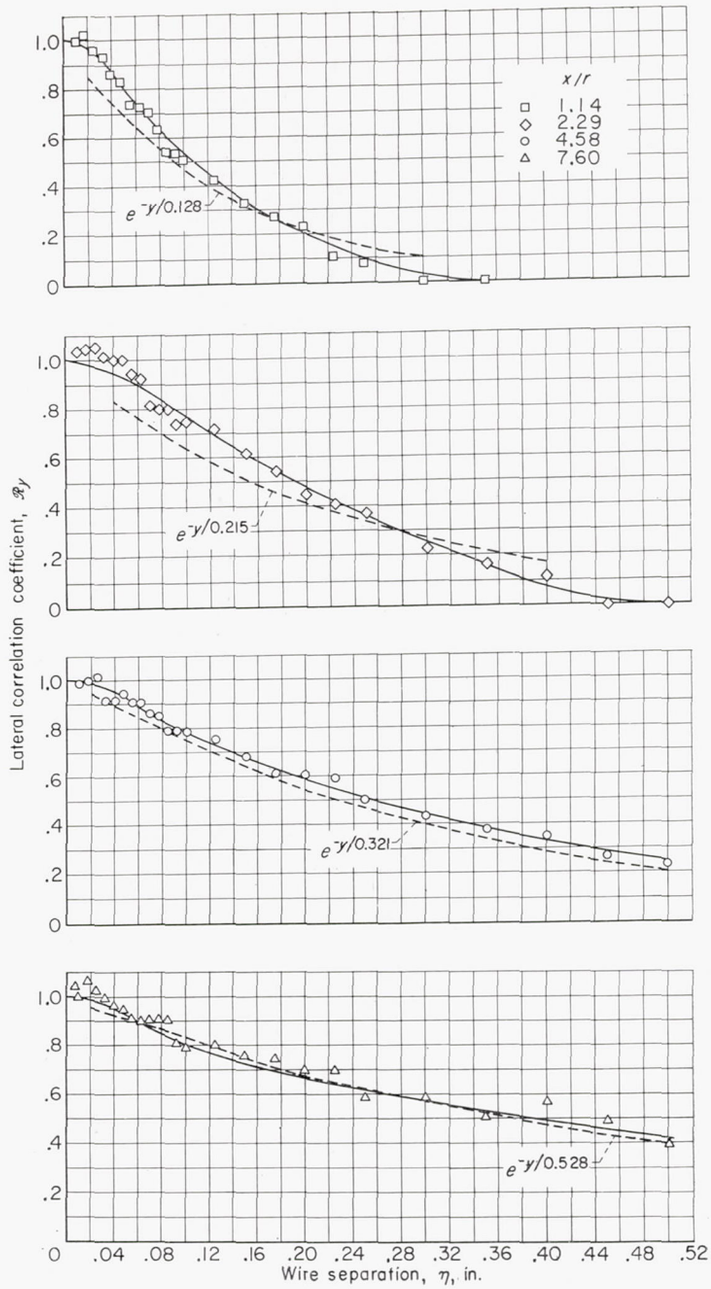

FIGURE 16.—Lateral velocity correlations. Distance from jet centerline y/r, 1.00; exit Mach number, 0.3; Reynolds number, 300,000.

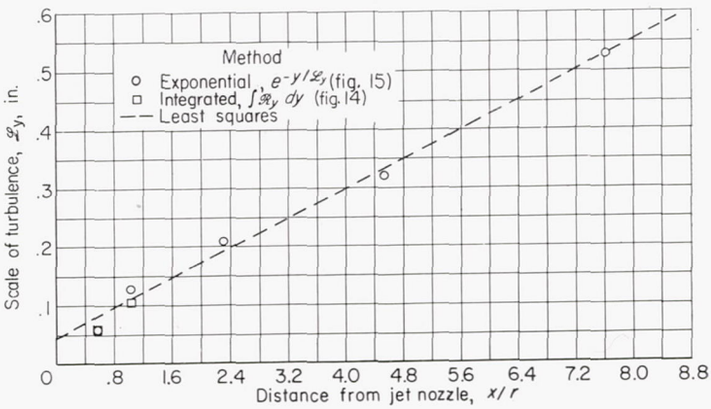

FIGURE 17.—Variation of lateral scale with distance from jet nozzle. Distance from jet centerline y/r, 1.00; exit Mach number, 0.3; Reynolds number, 300,000.

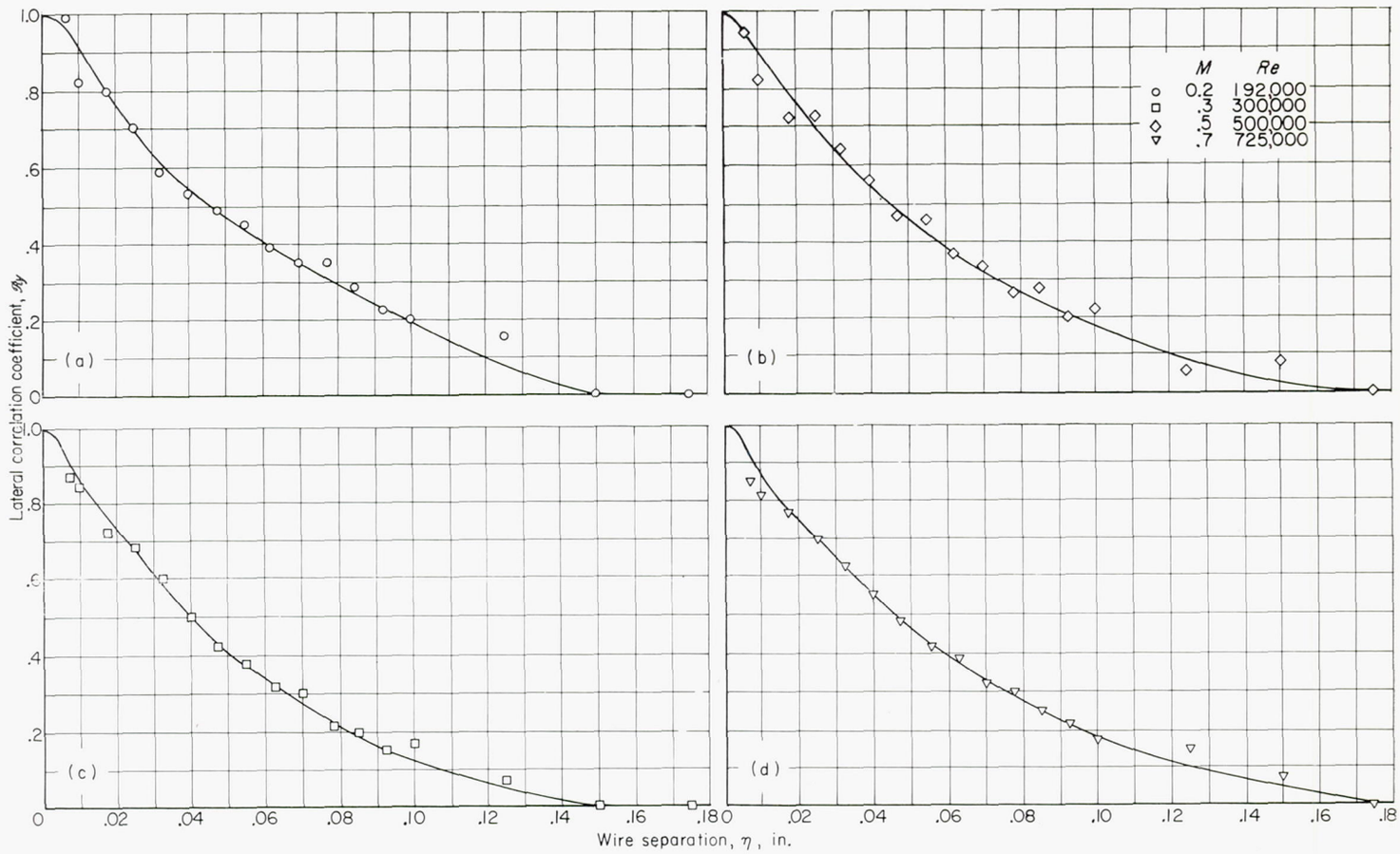

FIGURE 18.—Effect of exit Mach and/or Reynolds number on lateral velocity correlations. Distance from jet nozzle x/r, 0.57; distance from jet centerline y/r, 1.00.

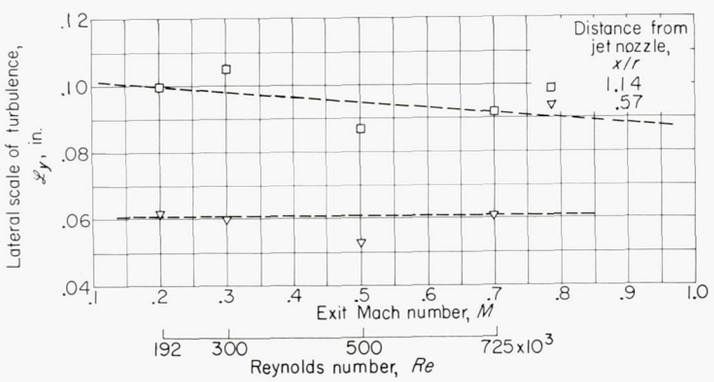

FIGURE 19.—Effect of exit Mach and/or Reynolds number on lateral scale of turbulence. Distance from jet centerline y/r, 1.00.

LATERAL SCALE OF TURBULENCE

The lateral correlation data of figures 15 and 16 for $y/r=1.00$ are compared in figure 17, where the lateral scale of turbulence is shown as a function of distance downstream of the nozzle. An exponential curve was faired through the data points of the correlation curves (fig. 16), and a representative value of the scale was obtained. The results show an approximately proportional increase of lateral scale with distance from the jet nozzle. The least-square line gives the relation

$$\mathcal{L}_y=0.036x+0.043 \tag{19}$$

which compares with

$$\mathcal{L}_y=0.028x \tag{20}$$

given in reference 8. Little, if any, variation of the lateral scale was found with distance from the jet centerline.

MACH AND/OR REYNOLDS NUMBER EFFECTS

In figure 18 are shown the effects of exit Mach and/or Reynolds number on the lateral correlation coefficient $\mathcal{R}_y$ as a function of wire separation for Mach numbers of 0.2, 0.3, 0.5, and 0.7. These curves show no variation of lateral correlation coefficient with Mach and/or Reynolds number and show clearly that there is little or no effect of Mach and/or Reynolds number on the lateral scale. Figure 19 summarizes the data of figure 18 and similar data for x/r of 0.57 and 1.14 at a fixed y/r of 1.00.

LONGITUDINAL CORRELATION COEFFICIENTS

The longitudinal correlations measured with two wires are given in figures 20 and 21. Figure 20 shows the variation of the longitudinal correlation coefficient $\mathcal{R}_x$ with distance across the mixing zone for x/r of 1.14. At the points near the core of the jet ($y/r<1$), strong periodic signals of approximately 8000 cps were encountered. Their presence causes the apparent scatter in the data of figures 20(g) to (i). The source of these disturbances is unknown, but the wavelength of the disturbance is approximately half the diameter of the jet nozzle. Perhaps transverse oscillations are responsible. Figure 21 shows the variation of the longitudinal correlation coefficient with distances from the jet nozzle of 1.14, 2.29, and 4.58.

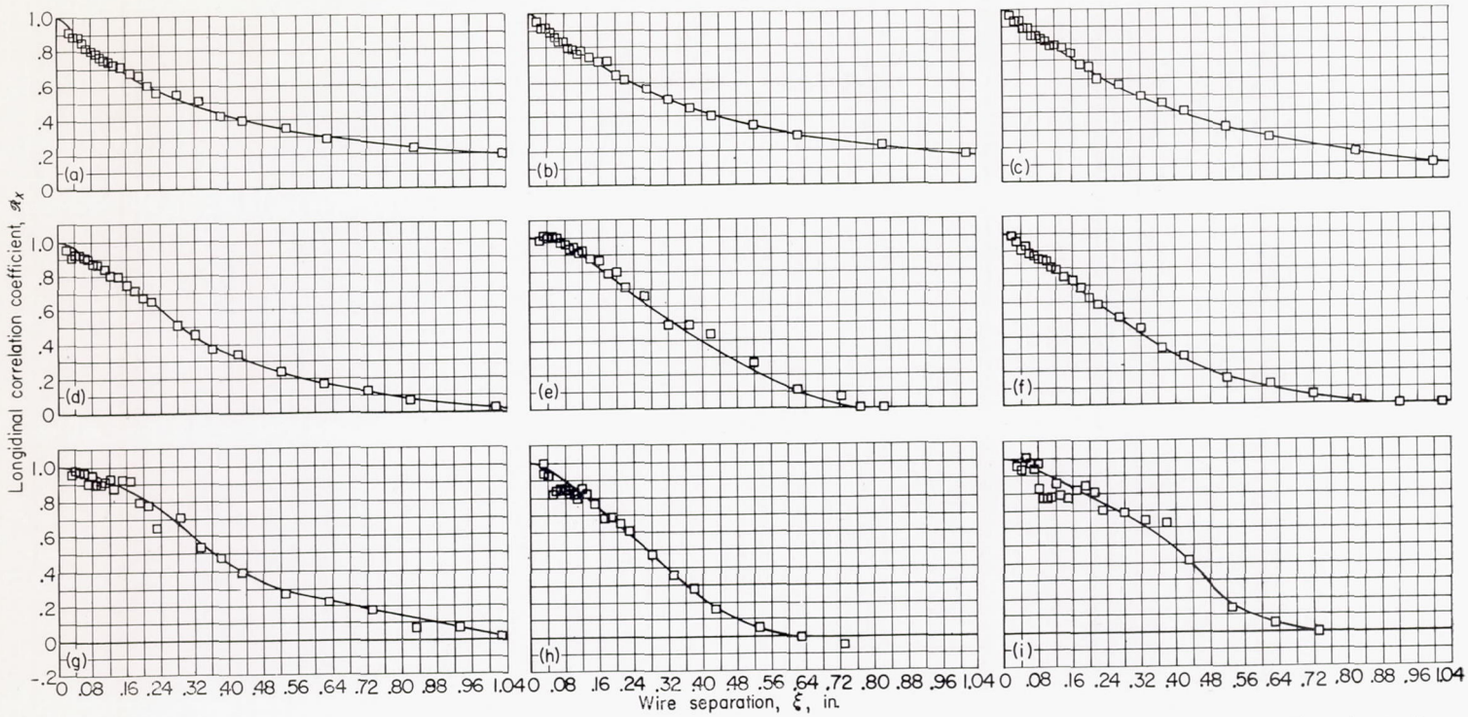

(a) Distance from jet centerline y/r, 1.20. (b) Distance from jet centerline y/r, 1.154. (c) Distance from jet centerline y/r, 1.103.
(d) Distance from jet centerline y/r, 1.051. (e) Distance from jet centerline y/r, 1.00. (f) Distance from jet centerline y/r, 0.949.
(g) Distance from jet centerline y/r, 0.897. (h) Distance from jet centerline y/r, 0.846. (i) Distance from jet centerline y/r, 0.794.

FIGURE 20.—Longitudinal velocity correlations. Distance from jet nozzle x/r 1.14; exit Mach number, 0.3; Reynolds number, 300,000.

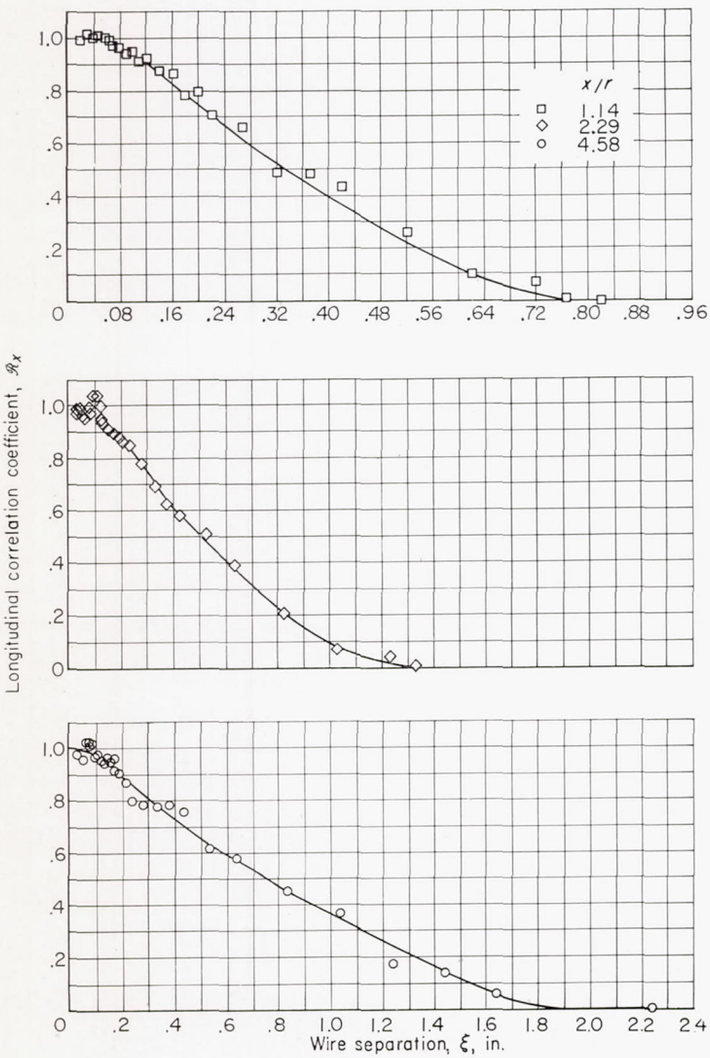

Inspection of figures 20 and 21 shows that the longitudinal correlation is affected by varying x/r and y/r. This effect will become more apparent when the longitudinal scale is evaluated from the area under the correlation curves; the variation is discussed in the section LONGITUDINAL SCALE OF TURBULENCE.

AUTOCORRELATIONS

The autocorrelation functions are presented in figures 22 and 23. Figure 22 shows the autocorrelation coefficient as a function of delay time in milliseconds for a fixed x/r value of 1.14 and for y/r values distributed as shown in figure 1. Figure 23 shows curves of autocorrelation coefficient against delay time for a fixed y/r of about 1.00 for several x/r values. Again, the effect of varying x/r and y/r will become apparent when the scale of turbulence is discussed. In figures 22 and 23 the influence of the periodic disturbances is exaggerated because of the size of the time-delay intervals. The 8000-cps sound wave is especially prominent, as well as another type of extraneous signal that resulted from floor vibrations due to heavy machinery in the building. For example, figures 22(g) and (h) show both types of interference. These wiggles are not present in figure 23, where the distribution with distance downstream of the nozzle of the jet is shown.

As has been pointed out, the autocorrelations can be converted to longitudinal correlations by certain relations of the mean flow. Figure 24 shows a comparison of the two measurements of the longitudinal correlation coefficient. The agreement is quite good, and the curves shown are typical of the measurements. The two-wire correlations

FIGURE 21.—Longitudinal velocity correlations. Distance from jet centerline y/r, 1.00; exit Mach number, 0.3; Reynolds number, 300,000.

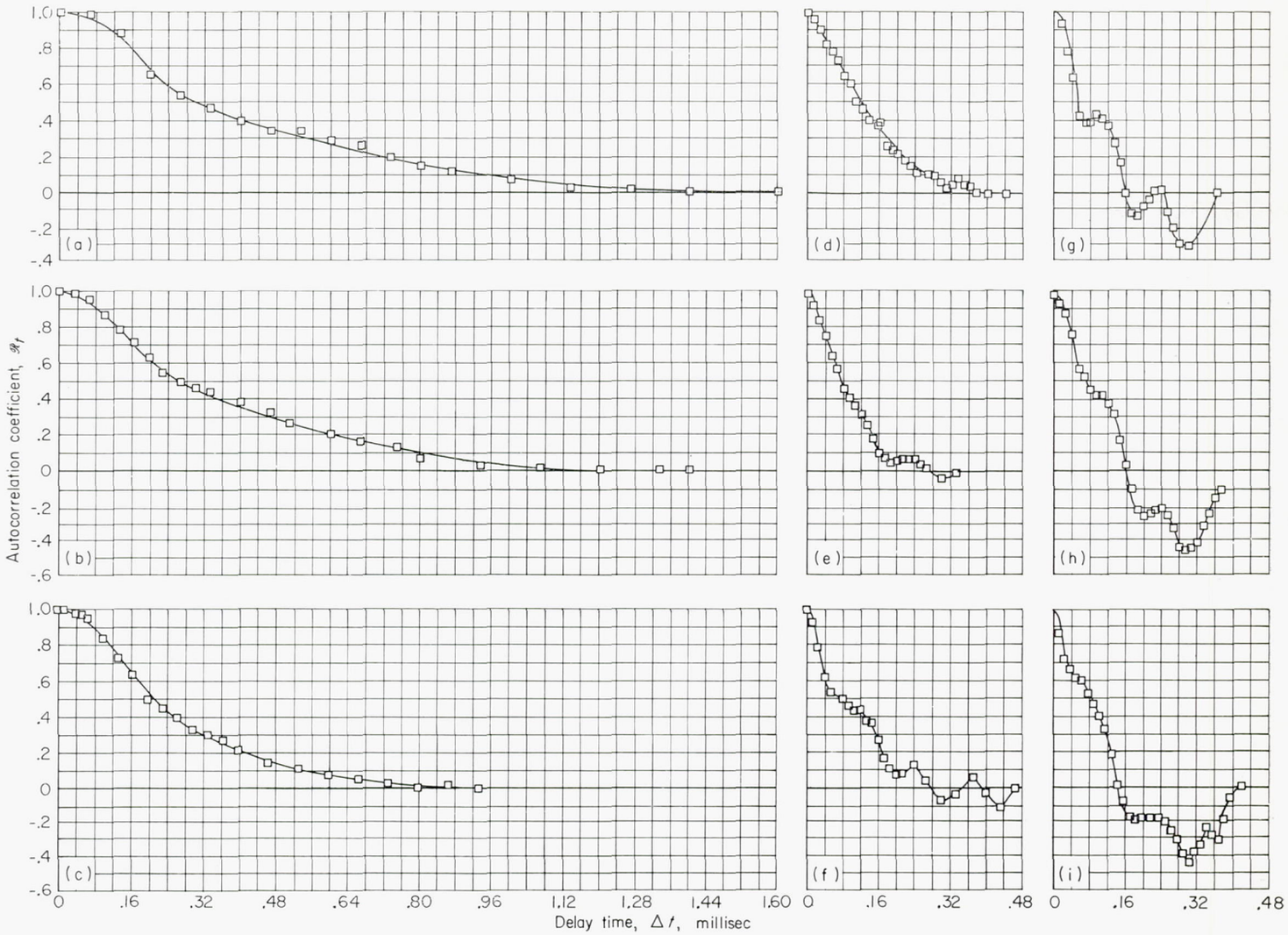

(a) Distance from jet centerline y/r, 1.206.
(b) Distance from jet centerline y/r, 1.154.
(c) Distance from jet centerline y/r, 1.103.
(d) Distance from jet centerline y/r, 1.051.
(e) Distance from jet centerline y/r, 1.00.
(f) Distance from jet centerline y/r, 0.949.
(g) Distance from jet centerline y/r, 0.897.
(h) Distance from jet centerline y/r, 0.846.
(i) Distance from jet centerline y/r, 0.794.

FIGURE 22.—Autocorrelations. Distance from jet nozzle x/r, 1.14; exit Mach number, 0.3; Reynolds number, 300,000.

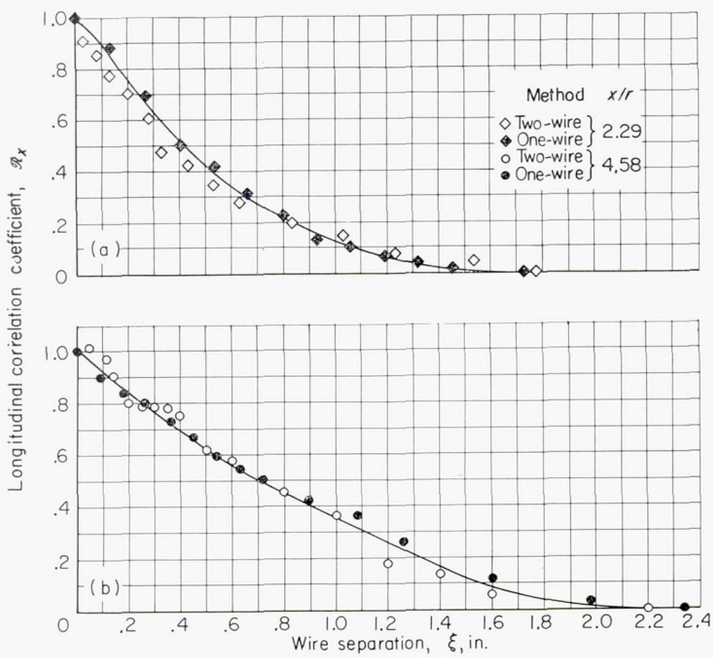

(a) Distance from jet centerline y/r, 1.103.
(b) Distance from jet centerline y/r, 1.00.

FIGURE 24.—Comparison of longitudinal velocity correlations from one- and two-wire methods.

were measured with the quarter-square method of multiplication using the average-square computer. The one-wire results were measured with the analog multiplier. If both measurements had been made with the analog multiplier, the agreement would probably be even better.

SPECTRA OF TURBULENCE

The spectra of the u-component of the turbulent velocity are shown in figures 25 and 26. Figure 25 shows the spectra for a fixed x/r value of 1.14 and a series of y/r values distributed as shown in figure 1. On the other hand, figure 26 presents the spectra for a fixed y/r value of approximately 1.00 and a series of x/r values. The change in the spectra with distance from the nozzle of the jet is primarily a shift of energy to lower frequencies as x/r increases. The effect of this increase will be discussed at the time the longitudinal scale of turbulence is considered.

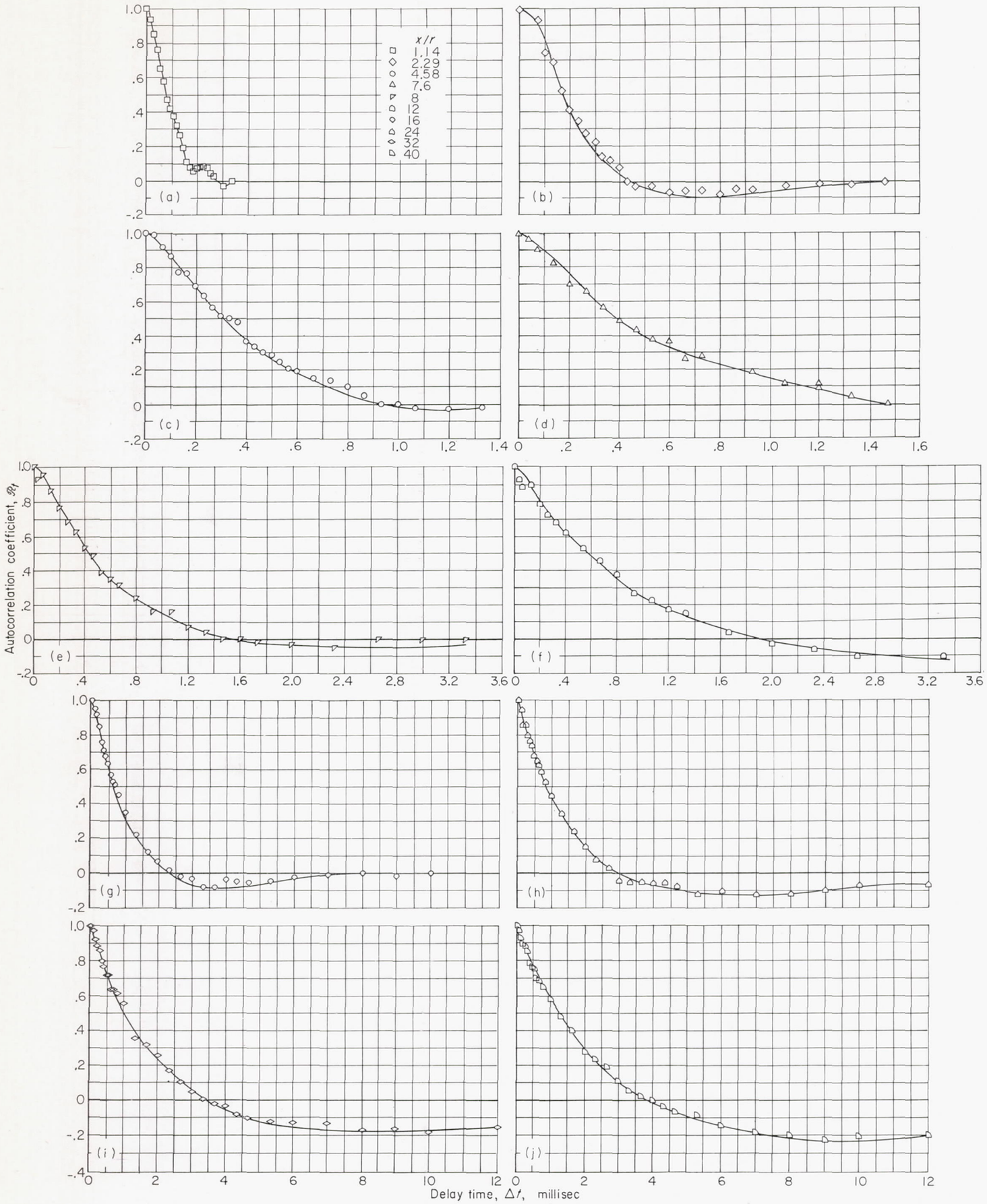

(a) to (f) Distance from jet centerline y/r, 1.00.
(g) to (j) Distance from jet centerline y/r, 1.028.

FIGURE 23.—Autocorrelations. Exit Mach number, 0.3; Reynolds number, 300,000.

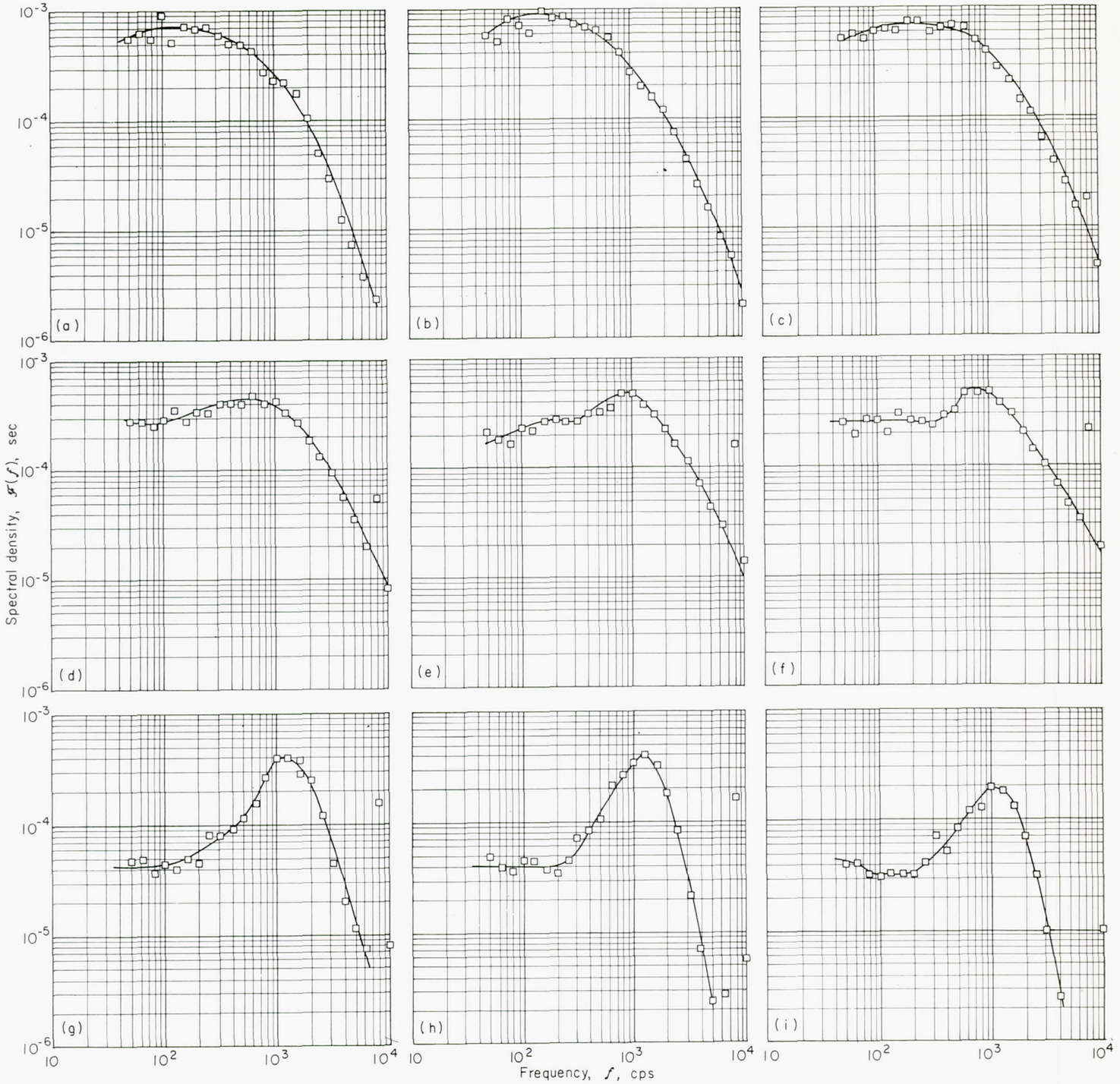

(a) Distance from jet centerline y/r, 1.206. (b) Distance from jet centerline y/r, 1.154. (c) Distance from jet centerline y/r, 1.103.
(d) Distance from jet centerline y/r, 1.051. (e) Distance from jet centerline y/r, 1.00. (f) Distance from jet centerline y/r, 0.949.
(g) Distance from jet centerline y/r, 0.846. (h) Distance from jet centerline y/r, 0.794. (i) Distance from jet centerline y/r, 0.743.

FIGURE 25.—Spectral density curves. Distance from jet nozzle x/r, 1.14; exit Mach number, 0.3; Reynolds number, 300,000.

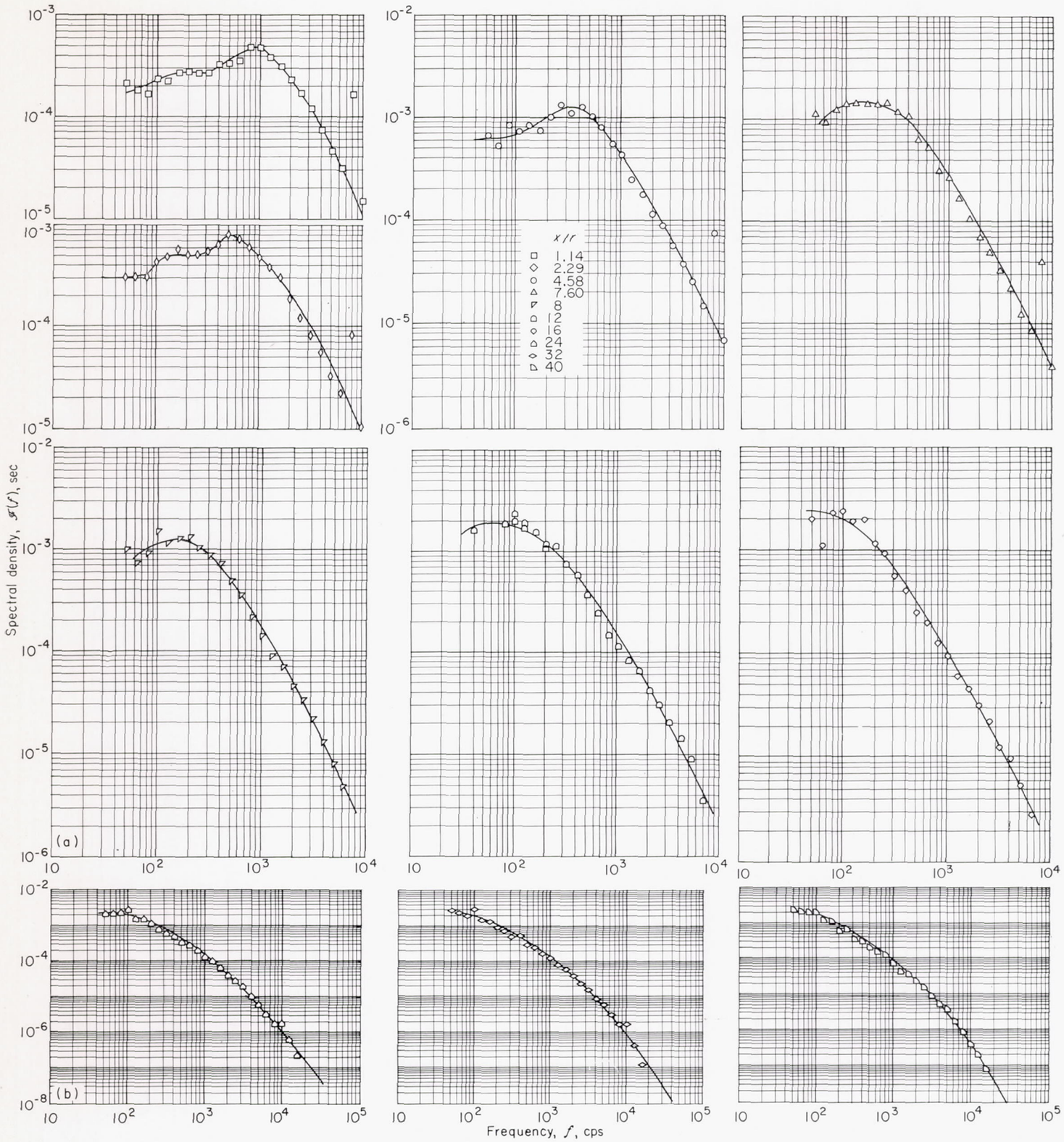

(a) Distance from jet centerline y/r, 1.00.
(b) Distance from jet centerline y/r, 1.028.

FIGURE 26.—Spectral density curves. Exit Mach number, 0.3; Reynolds number, 300,000.

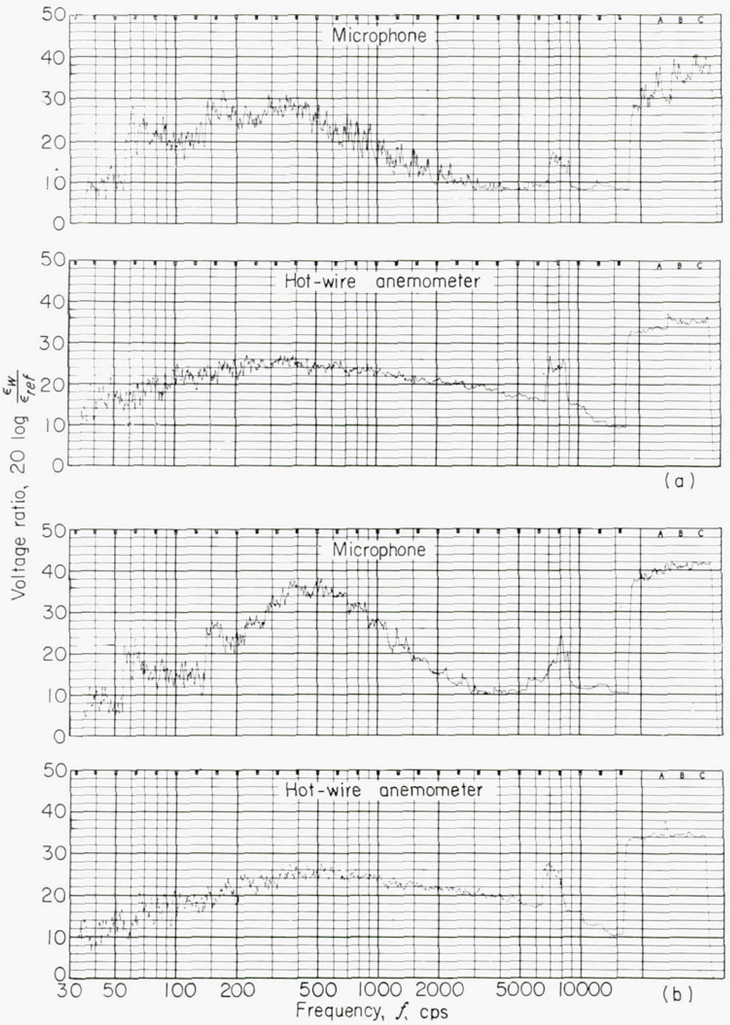

(a) Distance from jet nozzle x/r, 4.58.
(b) Distance from jet nozzle x/r, 7.60.

FIGURE 27.—Comparison of spectra obtained from a hot-wire anemometer and a microphone. Distance from jet centerline y/r, 1.00; exit Mach number, 0.3; Reynolds number, 300,000.

There is a marked change in the u spectra as the distance from the jet centerline y/r is changed. As the core of the jet is approached, a signal at approximately 8000 cps increases by more than an order of magnitude. This signal was believed to originate from a sound wave of that frequency.

In figure 27 are compared microphone spectra and hot-wire spectra recorded for two different values of x/r with the microphone displaced in the z-direction to remove it from the airstream. The presence of a strong signal at approximately 8000 cps, which can be seen on both sets of records, shows that a sound wave is indeed the source of the extraneous disturbance.

LONGITUDINAL SCALE OF TURBULENCE

The longitudinal scale of turbulence $\mathcal{L}_x$ was determined by integrating the area under the longitudinal correlation

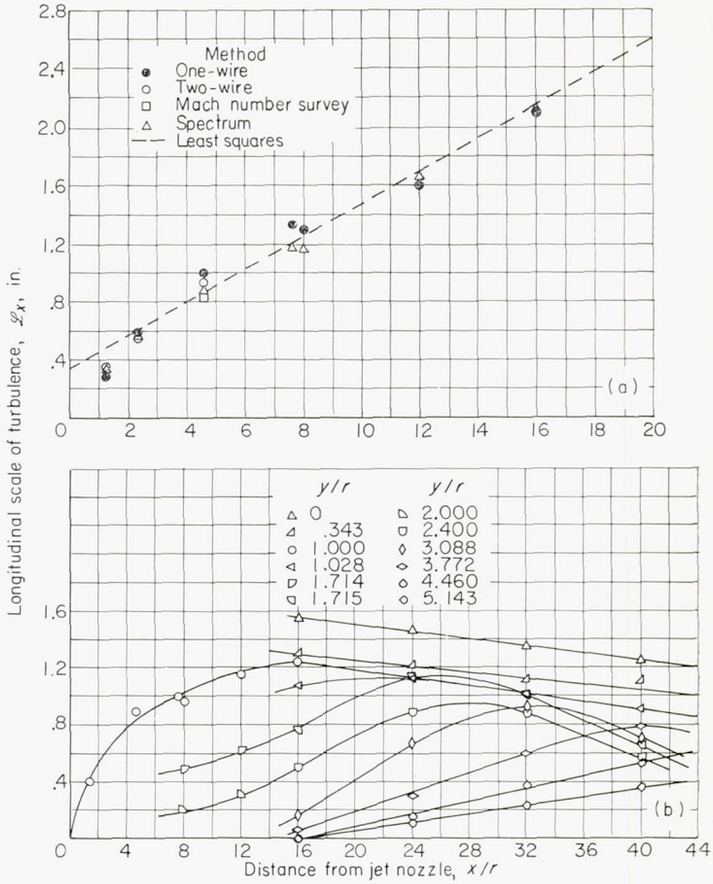

(a) Various methods.
(b) Various distances from jet centerline.

FIGURE 28.—Variation of longitudinal scale with distance from jet nozzle. Distance from jet centerline y/r, 1.00; exit Mach number, 0.3; Reynolds number, 300,000.

curves. The results are shown in figure 28. A straight line has been fitted to the data by the method of least squares (fig. 28(a)). This straight line represents the variation of the longitudinal scale quite well for distances from the jet nozzle less than 16 radii. In figure 28(b) the results are plotted for downstream distances as great as 40 jet radii and show clearly the decrease in longitudinal scale as the distance from the jet nozzle is increased beyond 16 radii.

The longitudinal scale of turbulence was evaluated by means of equation (13) and the spectral density curves of figures 25 and 26. It is obvious from equation (13) that

$$\mathcal{L}_x=\frac{\mathcal{F}(0)U_{loc}}{4} \tag{21}$$

Several schemes have been suggested to evaluate $\mathcal{F}(0)$, the spectral density function for zero frequency. For example, von Kármán (ref. 23) suggests that for small values of f an expression of the type

$$\mathcal{F}(f)=\frac{k_1}{(1+\pi^2k_1^2f^2)^{5/6}} \tag{22}$$

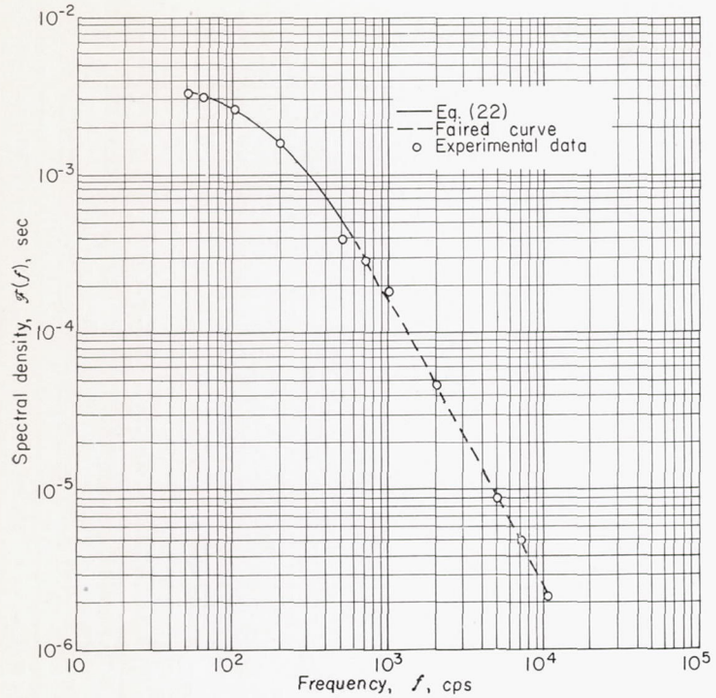

FIGURE 29.—Fitting spectral density data to empirical formula (ref. 23).

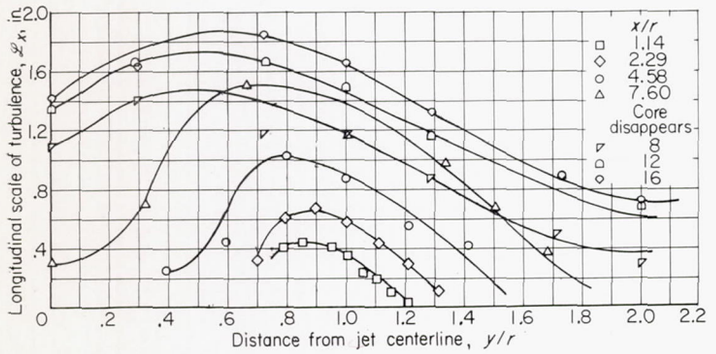

FIGURE 30.—Variation of longitudinal scale of turbulence across mixing zone. Exit Mach number, 0.3; Reynolds number, 300,000.

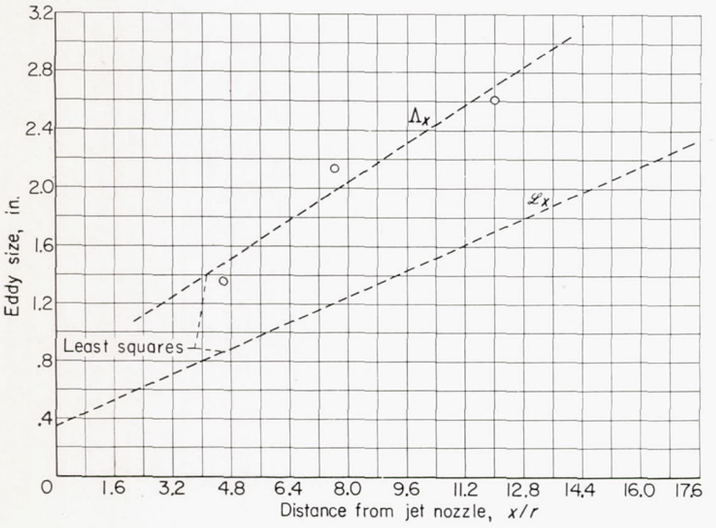

FIGURE 31.—Variation of eddy size with distance from jet nozzle (eq. (23)).

can be used to extrapolate to zero frequency. Corrsin and Uberoi (ref. 6) used this method to obtain the scale of turbulence. Figure 29 shows the result of fitting the data with a curve of the form of equation (22) for frequencies of 500 cps or less. It is seen that this method gives somewhat better results than equation (13).

If this method of extrapolation is used, a value of the scale of turbulence can be obtained. It is emphasized, however, that the two values of the scale obtained (by fitting the correlation curve with the best exponential and by finding the best fit for the spectral density curve according to equation (22)) are not necessarily the same. This particular example shows the relative inadequacy of the method of equation (21) for obtaining the scale of turbulence.

The method used in this report was simply to fair the best curve through the experimental data and estimate the maximum value of $\mathcal{F}(f)$. This value of $\mathcal{F}(f)$ is called the $\mathcal{F}(0)$ used in equation (21). This method gives values of $\mathcal{L}_x$ that agree well with the values obtained by integration of the correlograms, as is shown in figure 28(a), thus validating this method of selecting $\mathcal{F}(0)$. The values of $\mathcal{L}_x$ are plotted in figure 30.

Examination of figures 17 and 28(a) shows that $\mathcal{L}_x$ is somewhat more than twice as large as $\mathcal{L}_y$ at $x/r=8$. In both figures, the values of $\mathcal{L}_y$ and $\mathcal{L}_x$ for $x/r=1.14$ fall below the least-squares lines. The scatter about that line is small except for this point. Inspection of figures 28(a) and (b) shows that it may be possible to fit the data with some combination of a parabola up to $x/r=16$ and a straight line thereafter. This possibility suggests that the character of the turbulence changes at about that distance from the nozzle of the jet. In the mixing zone, the scale of turbulence is given by one relation, while the disappearance of the core results in an entirely different one.

This fact is also shown by figure 30, which gives the relation of the longitudinal scale to the distance from the centerline of the jet. As long as there is a core, the relation is definitely one type, which changes markedly upon the disappearance of the core. This change, however marked it may be, does not influence the position of the largest eddies ($\mathcal{L}_{x,max}$) near the y/r value of 0.7 to 0.8 for values of $x/r<16$.

An analysis of the correlograms and spectrograms was made using the equation

$$\Lambda_x = -\frac{x_0(1-\beta)}{\ln \beta} \tag{23}$$

The Λ scale of the turbulence was calculated by the methods outlined in appendix B. This Λ scale is different from that of the conventional scale $\mathcal{L}_x$, but the over-all picture is much the same. Figure 31 shows the variation of this Λ scale with distance from the jet nozzle. Here the variation is linear with x/r, as was shown in figure 28(a).

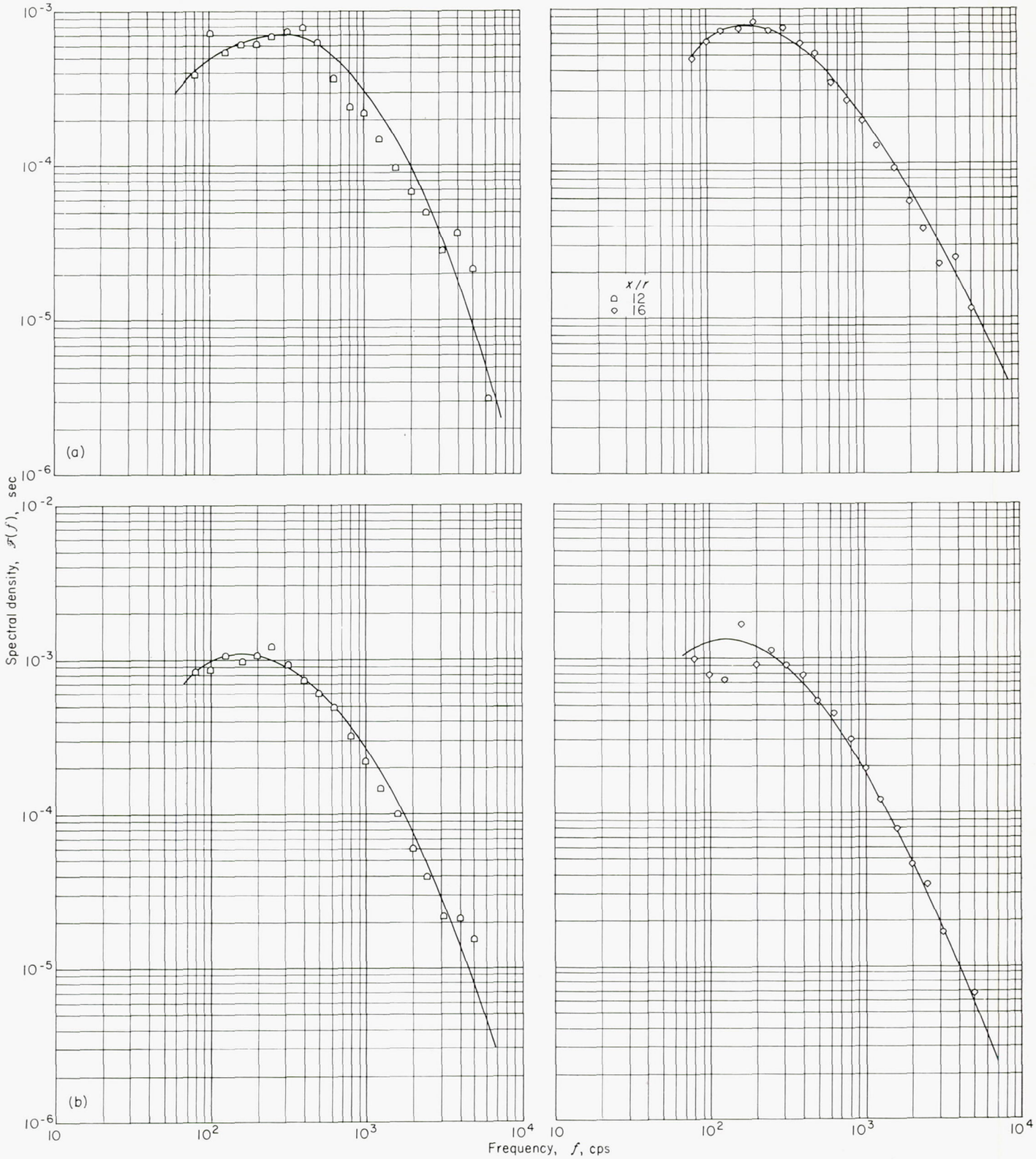

(a) Distance from jet centerline y/r, 0.
(b) Distance from jet centerline y/r, 1.00.

FIGURE 32.—Spectral density curves for v-component. Exit Mach number, 0.3; Reynolds number, 300,000.

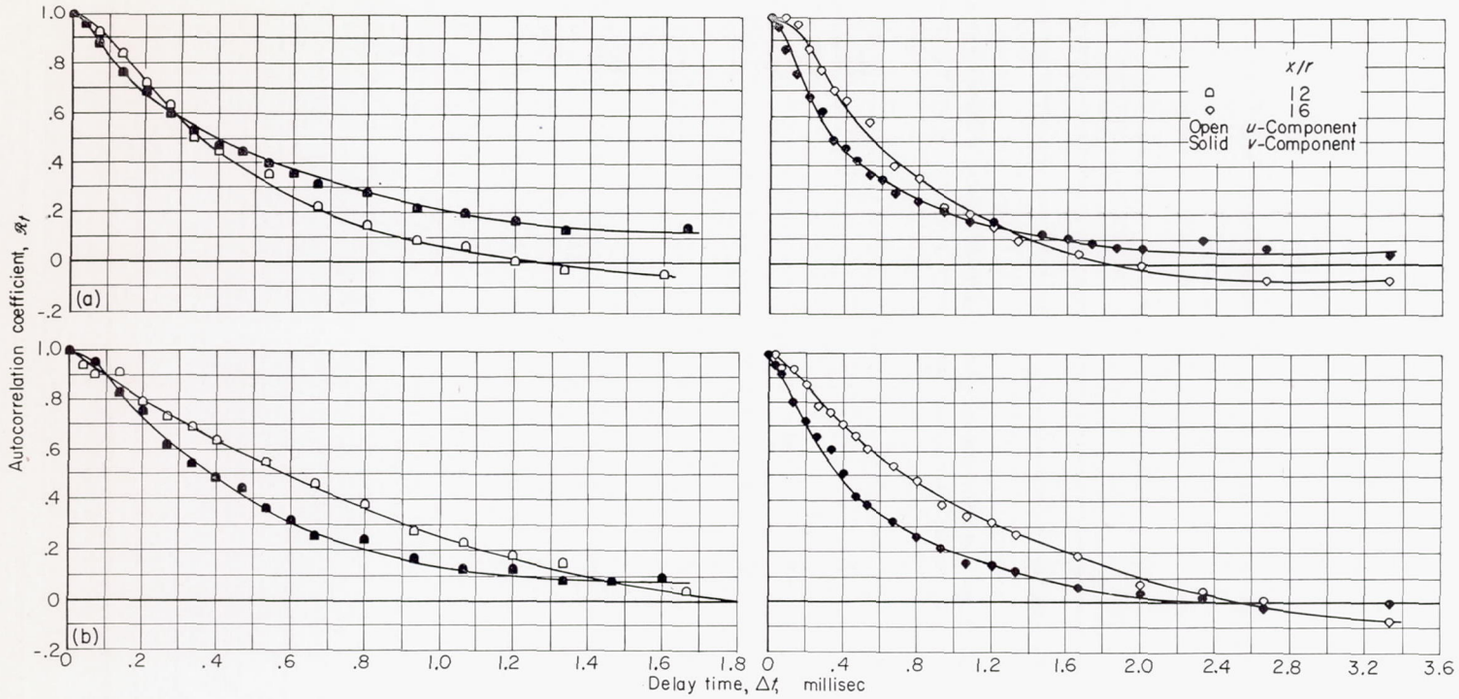

(a) Distance from jet centerline y/r, 0.
(b) Distance from jet centerline y/r, 1.00.

FIGURE 33.—Velocity autocorrelations of u- and v-components. Exit Mach number, 0.3; Reynolds number, 300,000.

CORRELATIONS AND SPECTRA OF v-COMPONENT OF TURBULENT VELOCITY

The correlations and spectra of the v-components of turbulence were obtained in order to compare them with those of the u-component. The spectra of the v-component of turbulence at four points in the jet are shown in figure 32. The spectra of the v-component of turbulence are different from the u-component in shape as well as in magnitude and frequency distribution. Figure 33 shows the autocorrelations of the v and the u velocity components at the same four points. These four curves indicate also the differences between the u- and v-components:

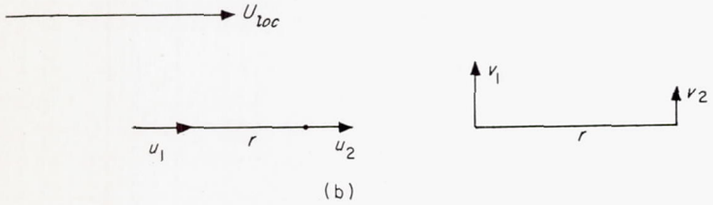

(b)

If the values of $\mathcal{R}_{x,u}$ and $\mathcal{R}_{y,v}$ are related by the following equation (ref. 10)

$$\mathcal{R}_{x,u}+\mathcal{R}_{y,v}=-\frac{x}{2}\frac{d\mathcal{R}_{x,u}}{dx} \tag{24}$$

then the turbulence is said to be isotropic. These u and v measurements, together with the v intensity measurements already discussed, show that the turbulence is not isotropic at distances from the jet less than 16 radii.

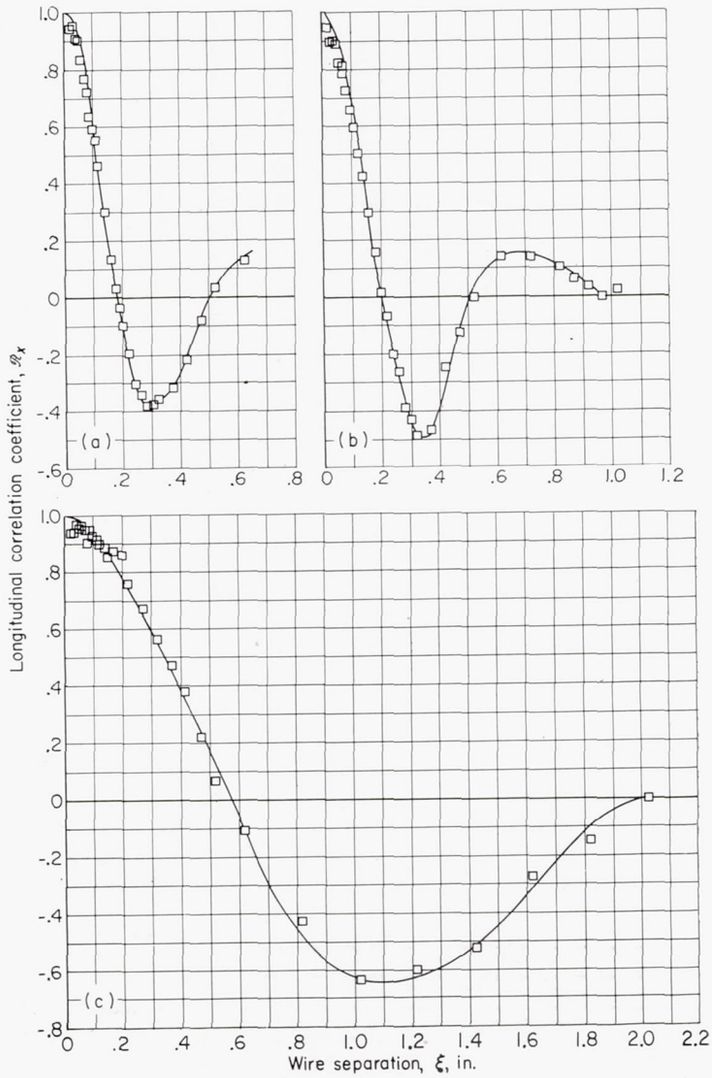

(a) Band-pass width, 4200 to 5800 cps; center frequency, 5000 cps.
(b) Band-pass width, 4800 to 5200 cps; center frequency, 5000 cps.
(c) Band-pass width, 900 to 1100 cps; center frequency, 100 cps.

FIGURE 34.—Longitudinal velocity correlations. Distance from jet nozzle x/r, 1.14; distance from jet centerline y/r, 1.00; exit Mach number, 0.3; Reynolds number, 300,000.

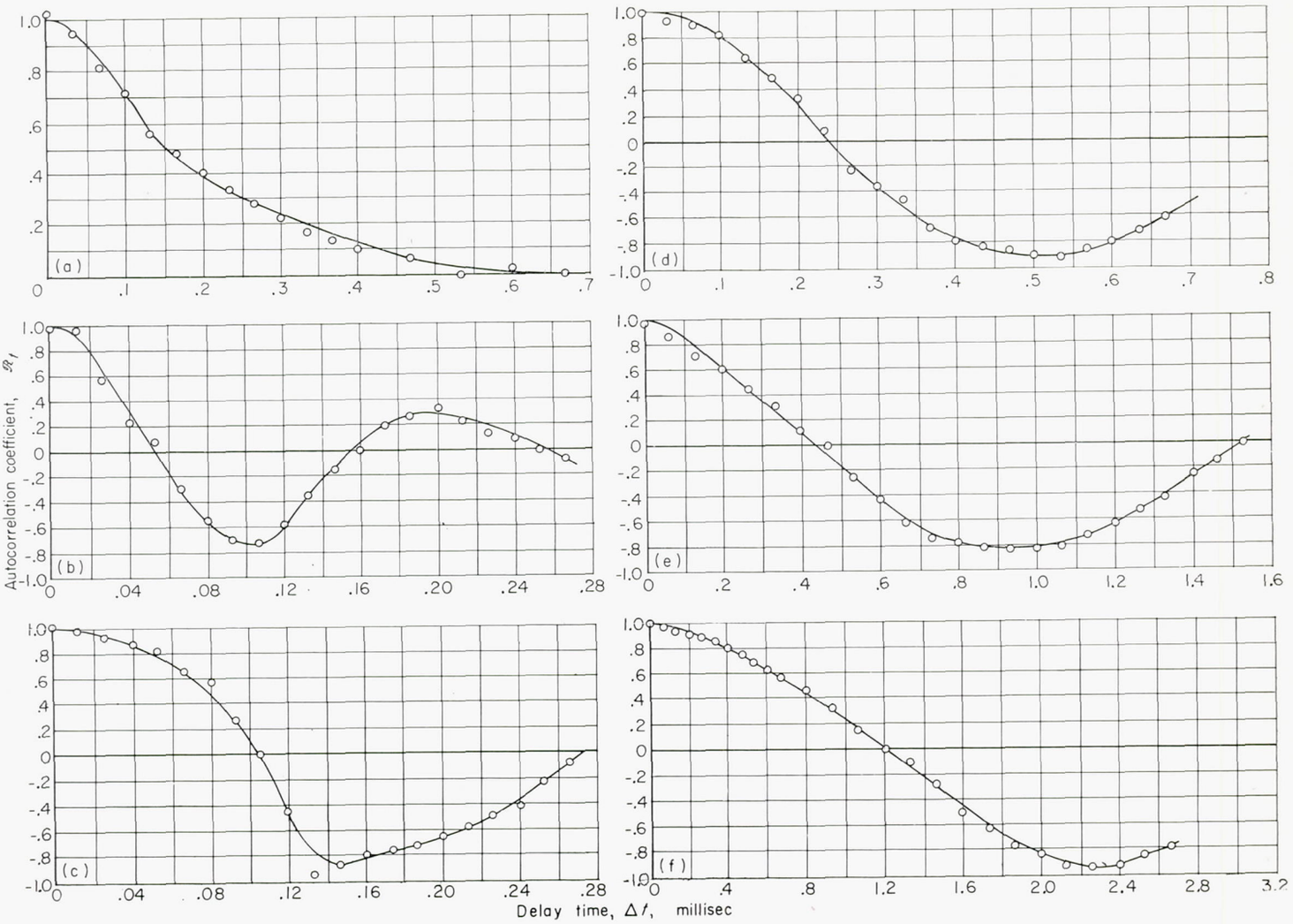

(a) No filter.
(b) Band-pass width, 4800 to 5200 cps.
(c) Band-pass width, 2900 to 3100 cps.
(d) Band-pass width, 900 to 1100 cps.
(e) Band-pass width, 480 to 520 cps.
(f) Band-pass width, 190 to 210 cps.

FIGURE 35.—Autocorrelations for specific band-pass frequencies. Distance from jet nozzle x/r, 4.58; distance from jet centerline y/r, 1.206; exit Mach number, 0.3; Reynolds number, 300,000.

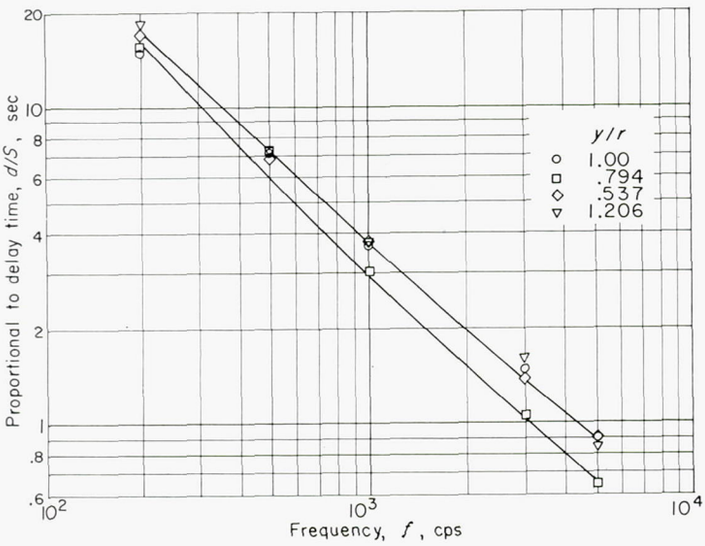

FIGURE 36.—Zero autocorrelation as function of frequency. Distance from jet nozzle x/r, 4.58; exit Mach number, 0.3; Reynolds number, 300,000.

CORRELATION WITH SPECIFIC BAND-PASS INPUTS

As an additional test of the autocorrelation technique for obtaining longitudinal correlation coefficients, the hot-wire signals were passed through electronic filters set to pass only specific bands of frequencies before they were fed to the correlation computers. Figures 34(a) and (b) show the effect of varying the band-pass width. The correlations do not change materially as the width of the band pass is changed by a factor of 4, except that the narrow band pass produces a greater negative correlation (ref. 21). Figure 34(c) shows the effect of changing the center frequency of the band pass.

In figure 35 are shown the autocorrelations for the experiments where the hot-wire signals were passed through electronic filters before being fed to the correlation computer. This figure illustrates the effect of varying the center frequency of the band pass, as did figure 34(c), and also shows clearly how the presence of the filters changes the correlations as measured (e.g., cf. fig. 35(a), for which no filter was used, with the other parts of fig. 35, for which the filters were used).

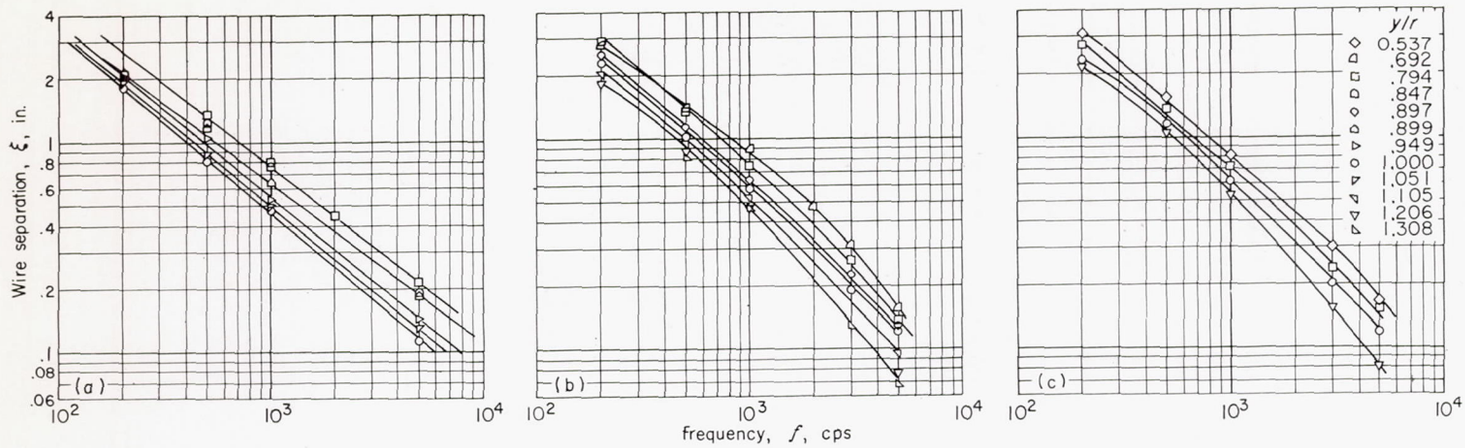

(a) Distance from jet nozzle x/r, 1.14. (b) Distance from jet nozzle x/r, 2.29. (c) Distance from jet nozzle x/r, 4.58.

FIGURE 37.—Zero longitudinal correlation distance as function of frequency. Exit Mach number, 0.3; Reynolds number, 300,000.

If the logarithm of the delay time for the first zero crossing of the filtered autocorrelation curve is plotted against the logarithm of the center frequency of the band pass (fig. 36), a straight line with a slope of -1 results. If the logarithm of the wire separation for zero longitudinal correlation is plotted against the logarithm of the center frequency of the band pass, a similar result should be obtained if the turbulent eddy has remained unchanged while passing the hot wires. That is, the eddy has been swept along unchanged with the velocity of the stream. Observation of figure 37 shows that these curves are nearly straight lines with a slope of -1. This is additional evidence that the relation $x=U_{loc}t$ holds very well for the turbulence patterns in the subsonic jet. Thus, the autocorrelation technique is a satisfactory one for studying the longitudinal correlations.

VARIATION OF SCALE OF TURBULENCE WITH MACH AND/OR REYNOLDS NUMBER

The effect of exit Mach and/or Reynolds number on the longitudinal scale was also investigated (fig. 38). As with the lateral scale (fig. 19), there was no variation of the longitudinal scale with Mach and/or Reynolds number.

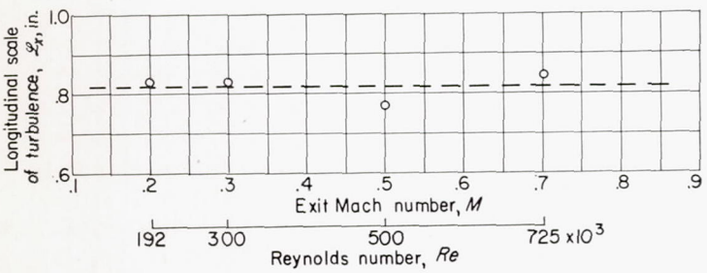

FIGURE 38.—Effect of exit Mach and/or Reynolds number on longitudinal scale of turbulence. Distance from jet nozzle x/r, 4.58; distance from jet centerline y/r, 1.00.

SUMMARY OF RESULTS

Hot-wire-anemometer measurements of the turbulence parameters—intensity, scale, correlation, and spectra—in a subsonic jet have been reported for a range of exit Mach numbers from 0.2 to 0.7 and for Reynolds numbers from 192,000 to 725,000, with the following results:

1. Near the nozzle of the jet (distances less than 4 or 5 jet diam downstream of the nozzle) the intensity of turbulence, expressed as a percent of core velocity, is a maximum at a distance of approximately 1 jet radius from the centerline and decreases slightly with increasing Mach and/or Reynolds number. At distances greater than 8 diameters, however, the maximum intensity moves out and decreases in magnitude until the turbulence-intensity profiles are quite flat and approaching similarity.

2. The lateral and longitudinal scales of turbulence are nearly independent of Mach and/or Reynolds number and, in the mixing zone near the jet, vary proportionally with distance from the jet nozzle. Farther downstream of the jet nozzle the longitudinal scale reaches a maximum and then decreases approximately linearly with distance. Near the nozzle the lateral scale is much smaller than the longitudinal and does not vary with distance from the centerline, while the longitudinal scale is a maximum at a distance from the centerline of about 0.7 to 0.8 of the jet radius. Farther downstream this maximum moves out from the centerline.

3. An analysis of the correlograms and spectra, which differs from the ordinary statistical approach, yields a "scale" which, while different in magnitude from the conventional, varies similarly to the ordinary scale and is easier to evaluate.

4. An autocorrelator using a magnetic tape recorder and a special playback instrument was used to measure the velocity autocorrelations. These autocorrelations were converted to longitudinal correlations that agreed well with the directly measured longitudinal correlations.

LEWIS FLIGHT PROPULSION LABORATORY
NATIONAL ADVISORY COMMITTEE FOR AERONAUTICS
CLEVELAND, OHIO, *April 24, 1956*

APPENDIX A

SYMBOLS

B	effective power band width
d	displacement of heads of playback instrument
$\mathcal{F}(f)$	spectral density function of $\overline{u^2}$
f	frequency
k	calibration constant
$\mathcal{L}$	scale of turbulence
M	exit Mach number
N	number of db taken from strip chart
$\mathcal{R}$	correlation coefficient
Re	Reynolds number
r	jet radius
S	tape speed
t	time
Δt	delay time
U	mean stream velocity
u,v,w	fluctuating, components of velocity in x-, y-, and z-directions, respectively
x,y,z	right-hand coordinate system with x-axis coinciding with jet centerline
β	nondimensional parameter related to cut-off frequencies of spectrum by eq. (B5)
ϵ	fluctuating component of hot-wire voltage
ζ,η	wire separation in x- and y-directions, respectively
Λ	characteristic eddy size
ω	angular frequency

Subscripts:

b	band of frequencies
c	core
f	frequency
l	lower cut-off
loc	local
max	maximum
min	minimum
p	peak
ref	reference
t	time
tot	total spectrum of all frequencies
u	upper cut-off
w	wire
x	longitudinal
y	lateral
z	lateral
1,2	points in stream

Superscripts:

—	average
$'$	root-mean-square
*	characteristic value

APPENDIX B

ANALYSIS OF TURBULENCE SPECTRA AND AUTOCORRELOGRAMS

The analysis of the data from the hot-wire anemometers is most easily accomplished by means of the power spectrum of the turbulence and the autocorrelation technique, as explained in the EXPERIMENTAL PROCEDURE section. The details of this analysis are interesting also. The correlation fitting function

$$\mathcal{R}_x=\frac{e^{-x/\Lambda_x}-\beta e^{-\beta x/\Lambda_x}}{1-\beta} \tag{14a}$$

or

$$\mathcal{R}_t=\frac{e^{-\omega^* t}-\beta e^{-\beta\omega^* t}}{1-\beta} \tag{14b}$$

can be transformed to the spectral density function $\mathcal{F}(f)$ as follows:

$$\mathcal{F}(f)=\frac{4}{U_{loc}}\int_0^\infty \mathcal{R}_x \cos\frac{2\pi f x}{U_{loc}}\,dx \tag{B1a}$$

or

$$\mathcal{F}(f)=4\int_0^\infty \mathcal{R}_t \cos 2\pi f t\,dt \tag{B1b}$$

The resulting expression for $\mathcal{F}(f)$ is

$$\mathcal{F}(f)=\frac{1+\beta}{4f^*}\frac{\left(\frac{f}{f^*}\right)^2}{\left[1+\left(\frac{f}{f^*}\right)^2\right]\left[\beta^2+\left(\frac{f}{f^*}\right)^2\right]} \tag{17}$$

This equation for $\mathcal{F}(f)$ has many interesting features. Consider, for instance, sketches (c) and (d). The typical correlogram shows a zero crossing (t_0) and a minimum value. These two quantities and the following equations for $\mathcal{R}_{t,min}$ and ω^*

$$\mathcal{R}_{t,min}=-\beta^{\frac{1+\beta}{1-\beta}} \tag{B2}$$

$$\omega^*=\frac{\ln\beta}{t_0(\beta-1)} \tag{B3}$$

give values for β and ω^* from the experimental correlogram. With these values the spectral density curve can be calculated from equation (17).

An alternate procedure is to work with the experimental spectral density curve. If the low-frequency part of the curve has been obtained with sufficient accuracy, the values of the low- and high-frequency cut-offs (f_l and f_u) can be obtained from the spectrum. These two values with the equations

$$\frac{f_l}{f_u}=\frac{\beta}{(1+\beta)^2} \tag{B4}$$

and

$$f_u=\frac{(1+\beta)\omega^*}{2\pi} \tag{B5}$$

give values for β and ω^* from the experimental spectrum. With these values the correlogram can be calculated from equation (14a) or (14b).

In actual practice the low-frequency part of the spectrum is seldom defined with sufficient accuracy to use the alternate method proposed here. But the correlograms are generally well defined and are easily used as outlined.

If a family of curves of $\mathcal{F}(f)$ for a series of values of β is plotted as shown in figure 39, spectrum fitting curves result that differ from experimental curves only by multiplicative constants. This family of curves can be used as a grid and placed over the experimental data and a best fit obtained. The value of β, therefore, is easily determined. With this value of β and the zero crossing of the correlogram t_0, the value of ω^* can be obtained from equation (B3).

With the values of β and ω^* the spectrum can be calculated by means of equation (17), or Λ_x can be evaluated by means of equation (16).

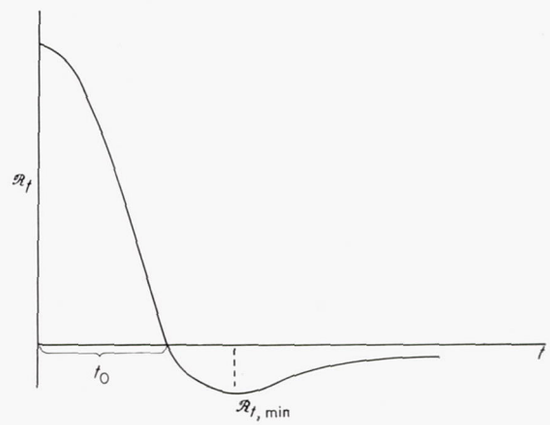

(c)

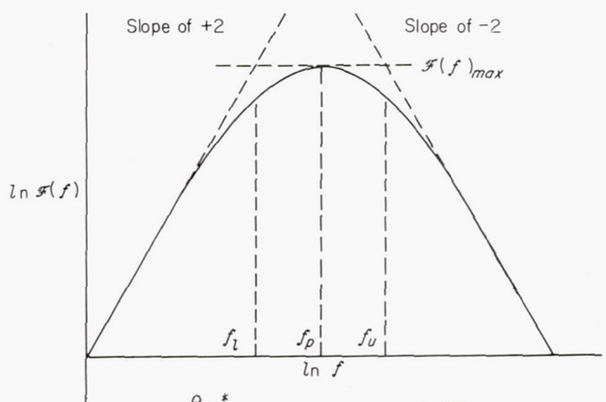

$f_l = \frac{\beta\omega^*}{1+\beta}$ $\qquad f_p = \omega^*\sqrt{\beta}$

$f_u = (1+\beta)\omega^*$ $\qquad \mathcal{F}(f)_{max} \approx \frac{2}{\pi(\beta+1)\omega^*}$

(d)

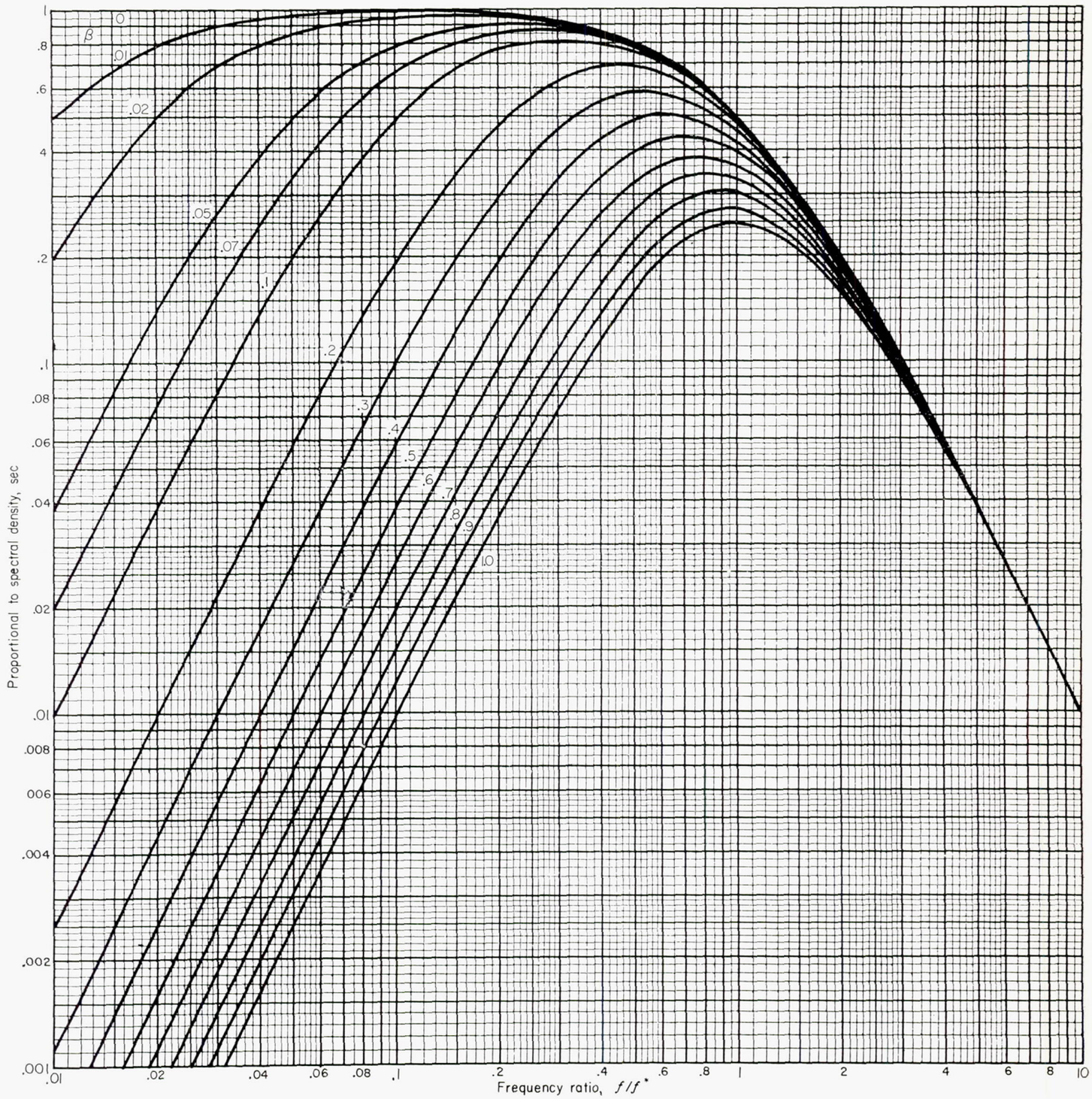

FIGURE 39.—Spectrum fitting curves (eq. (B2)).

REFERENCES

1. Lighthill, M. J.: On Sound Generated Aerodynamically. 1. General Theory. Proc. Roy. Soc. (London), ser. A, vol. 211, no. 1107, Mar. 20, 1952, pp. 564–587.
2. Proudman, I.: Generation of Noise by Isotropic Turbulence. Proc. Roy. Soc. (London), ser. A, vol. 214, 1952, pp. 119–132.
3. Mawardi, O. K., and Dyer, I.: On Noise of Aerodynamic Origin. Jour. Acoustic Soc. Am., vol. 25, no. 3, May 1953, pp. 389–394.
4. Kuethe, Arnold M.: Investigation of the Turbulent Mixing Regions Formed by Jets. Jour. Appl. Mech., vol. 2, no. 3, Sept. 1935, pp. A87–A95.
5. Corrsin, Stanley: Investigation of Flow in an Axially Symmetrical Heated Jet of Air. NACA WR W–94, 1943. (Supersedes NACA ACR 3L23.)
6. Corrsin, Stanley, and Uberoi, Mahinder S.: Further Experiments on the Flow and Heat Transfer in a Heated Turbulent Air Jet. NACA Rep. 998, 1950. (Supersedes NACA TN 1865.)
7. Corrsin, Stanley, and Uberoi, Mahinder S.: Spectra and Diffusion in a Round Turbulent Jet. NACA Rep. 1040, 1951. (Supersedes NACA TN 2124.)
8. Liepmann, Hans Wolfgang, and Laufer, John: Investigations of Free Turbulent Mixing. NACA TN 1257, 1947.
9. Taylor, G. I.: Statistical Theory of Turbulence, pts. I–IV. Proc. Roy. Soc. (London), ser. A, vol. 151, no. A873, Sept. 2, 1935, pp. 421–478; pt. V, ser. A, vol. 156, Aug. 17, 1936, pp. 307–317.
10. Dryden, Hugh L.: A Review of the Statistical Theory of Turbulence. Quarterly Appl. Math., vol. 1, no. 1, Apr. 1943, pp. 7–42.
11. Laurence, James C., and Landes, L. Gene: Auxiliary Equipment and Techniques for Adapting the Constant-Temperature Hot-Wire Anemometer to Specific Problems in Air-Flow Measurements. NACA TN 2843, 1952.
12. Sandborn, Virgil A.: Experimental Evaluation of Momentum Terms in Turbulent Pipe Flow. NACA TN 3266, 1955.
13. Schubauer, G. B., and Klebanoff, P. S.: Theory and Application of Hot-Wire Instruments in the Investigation of Turbulent Boundary Layers. NACA WR–86, 1946. (Supersedes NACA ACR 5K27.)
14. Mickelsen, William R., and Laurence, James C.: Measurement and Analysis of Turbulent Flow Containing Periodic Flow Fluctuations. NACA RM E53F19, 1953.
15. Dryden, H. L., and Kuethe, A. M.: The Measurement of Fluctuations of Air Speed by the Hot-Wire Anemometer. NACA Rep. 320, 1929.
16. Favre, A.: Mesures Statistiques de la Corrélation dans le Temps. Premieres applications á l'étude des mouvements turbulents en soufflerie. Pub. No. 67, Office Nat. d'Études et de Recherches Áero., 1953.
17. Hastings, A. E., and Meade, J. E.: A Device for Computing Correlation Functions. Rev. Sci. Instr., vol. 23, no. 7, July 1952, pp. 347–349.
18. Callaghan, Edmund E., Howes, Walton L., and Coles, Willard D.: Near Noise Field of a Jet-Engine Exhaust. II—Cross Correlation of Sound Pressures. NACA TN 3764, 1956.
19. Mickelsen, William R.: An Experimental Comparison of Lagrangian and Eulerian Correlation Coefficients in Homogeneous Isotropic Turbulence. NACA TN 3570, 1955.
20. Taylor, G. I.: The Spectrum of Turbulence. Proc. Roy. Soc. (London), ser. A, vol. 164, Feb. 18, 1938, pp. 476–490.
21. Dryden, Hugh L., Schubauer, G. B., Mock, W. C., Jr., and Skramstad, H. K.: Measurements of Intensity and Scale of Wind-Tunnel Turbulence and Their Relation to the Critical Reynolds Number of Spheres. NACA Rep. 581, 1937.
22. Pai, Shih-I.: Fluid Dynamics of Jets. D. Van Nostrand Co., Inc., 1954.
23. von Kármán, Theodore: Progress in the Statistical Theory of Turbulence. Proc. Nat. Acad. Sci., vol. 34, no. 11, Nov. 15, 1948, pp. 530–539.
24. Taylor, John F., Grimmett, H. L., and Comings, E. W.: Turbulent Mixing in a Isothermal Free Jet. Tech. Rep. No. 2, Univ. of Ill., Nov. 15, 1948. (Contract N6-ori-71, Task Order XI, Office Naval Res., Navy Dept.)

U. S. GOVERNMENT PRINTING OFFICE: 1957